Universidad de Sevilla

Westfälische Wilhelms-Universität Münster

Master Thesis

Dielectron production in p-p collisions with PYTHIA8 event generator

Pablo Pérez Maroto

First supervisor (WWU): Prof. Dr. Anton Andronic

Second supervisor (WWU): Apl. Prof. Dr. Christian Klein-Bösing

US supervisor: Carlos Guerrero Sánchez

21.12.2020

Todo es de color.

Triana

Acknowledgements
Agradecimientos

I would like to mention all the people without whom this thesis would not have come to fruition, for one reason or another. In the first place, I would like to thank Prof. Anton Andronic and Prof. Christian Klein-Bösing for accepting me in their group and for giving me their trust. Thanks especially to Anton for his guidance and advice, essential to finish the job. I would like to thank also Alexander Kappes for his invaluable help in the hard task of finding accommodation in Münster. Thanks to Ailec, Jan and Tabea for welcoming me in your office and solving all my questions.

I would like to thank all the Kernphysik Institut IT team, especially Katharina Garner for writing and keeping the "PYTHIA train" working and improving it on a daily basis. Without her work I would not have been able to performing the simulations of the thesis. Thanks to the rest of people of my group and the Institut for their kindness along the corridors.

Me gustaría agradecer a todos los profesores que he tenido la suerte de conocer a lo largo de la carrera y del máster, por despertar en mí la pasión hacia algo tan bonito como es la Física Nuclear y la Física en general. Gracias especialmente a Pepe Arias por haberme animado a emprender este viaje. Gracias también a Joaquín Ramírez Rico por su ayuda con todo lo relacionado con este programa ERASMUS tan peculiar por los tiempos que nos ha tocado vivir. Gracias a Carlos Guerrero por haber comprendido mi situación y permitirme empezar el doctorado desde Alemania.

Es probable que sin la companía de Dani, Lucas y Fernando tampoco me hubiese atrevido a venir hasta aquí. Desde luego, el "confinamiento" hubiese sido mil veces más difícil sin ellos, así que gracias por eso. Mencionar también a todas las personas y/o personajes que he ido conociendo estos meses en Münster, gracias a los cuales me llevo incontables anécdotas y buenos momentos.

Por último, no me olvido de mis padres, hermanas, abuelos y el resto de mi familia. Gracias por darme los ánimos necesarios para atreverme a hacer esto. Ojalá que el mundo no tarde en volver a la calma y podamos estar todos juntos de nuevo.

Alma, eres la persona más valiente que he conocido. No ha sido fácil, pero ya sabes por lo que estamos trabajando. Gracias, gracias y gracias.

Abstract

In this thesis the dielectron (electron-positron pair) production cross section in proton-proton collisions has been simulated as a function of their invariant mass and their transverse momentum, for an energy of $\sqrt{s} = 13$ TeV and $\sqrt{s} = 5.02$ TeV. These have been carried out using PYTHIA8 event generation. A series of studies have been conducted on how to extract the cross section, first by directly using the information provided by this software and then by imitating the signal extraction methods used with real experimental data. The effect on these simulations of the combinatorial background and photon conversion pairs has also been investigated.

Resumen

En este trabajo se ha simulado la sección eficaz de la producción de dielectrones (pares electrón-positrón) en colisiones protón-protón en función de la masa invariante de los mismos y su momento transversal, para una energía de $\sqrt{s} = 13$ TeV y $\sqrt{s} = 5.02$ TeV. Estas se han llevado a cabo mediante el programa de generación de eventos PYTHIA8. Se han realizado una serie de estudios atendiendo al modo de extraer la sección eficaz, primero utilizando directamente la información proporcionada por este software y después imitando los métodos de extracción de señal utilizados con datos experimentales reales. Así mismo, se ha investigado el efecto en estas simulaciones del fondo de combinatoria y de los pares de conversión fotónica.

Contents

1 Introduction

Mankind has always wondered about the nature and structure of the Universe we inhabit. Millennia of evolution and development has made it possible to offer an explanation to these concerns at a level never imagined before. On one side, the theoretical and mathematical progress that resulted in the Standard Model of particle physics has provided the tools and framework to describe the Universe at its smallest scale. On the other, an outstanding engineering work has led to the construction of particle accelerators with a huge power, like the Large Hadron Collider located at CERN. With these machines we can check if those theory predictions are indeed true and even make unexpected discoveries that imply new challenges for science.

One of the main experiments of LHC is ALICE. With this detector the goal is to study the so-called quark-gluon plasma (QGP). QGP is the hot and dense medium formed when two heavy nuclei collide at ultra-relativistic energies. Is crucial to understand the creation and evolution stages of this medium, because it can provide a large amount of information about the quarks that form matter and the interaction between them. Because of its design and the energies provided by the LHC is the perfect place to investigate these issues.

Due to their properties, dielectron (e^+e^- pairs) are used as a probe in the collisions to study QGP. Is crucial to understand very well the dielectron production in proton-proton collisions to, then, clarify the leptonic production in nuclei collisions. Recently the possibility of the creation of this thermalized medium in high-multiplicity p-p collisions is being taken into account [1], so it adds relevance to the matter.

Another motivation for the study of dielectron is charmonium production. Charmonium is a particle made of a charm-anticharm quark pair, and its most common state is the J/ψ meson. Is a remarkable particle because its experimental discovery in 1974 [2] resulted in the confirmation of the existence of a fourth quark flavour. The finding was made by two different groups simultaneously in the known as "November Revolution" of particle physics. The main channel chosen to select charmonia in a collision is the dielectron channel $J/\psi \to e^+e^-$, so a profound understanding of dielectron spectrum is vital, because it will be the major source of background in the charmonium signal.

In this thesis this will be carried out through simulations with PYTHIA8. To perform a real exhaustive investigation one should take the data obtained in PYTHIA and do a

Geant4 (or any other similar software) analysis, to really see how the ALICE detector would respond. We are going to pass over this part of the analysis, so the results will not be entirely realistic, but as a first approach and at the level of this thesis this will be enough. Anyway the results will be a very good approximation.

This thesis is structured as follows: after this brief introduction, a few theoretical ideas about the Standard Model and other concepts that appear in the thesis will be covered in Chapter 2. In Chapter 3 a short description of the ALICE experiment will be shown, and a few notions about the processes simulated by PYTHIA will be displayed in Chapter 4. The results of the simulations will be presented in Chapter 5, followed by a summary and an outlook for possible future investigations in Chapter 6. During this thesis, unless specified otherwise, when we mention "electrons" we are referring to electrons and positrons equally. In addition, we will use $c = \hbar = 1$ for simplicity.

2 Theoretical background

In this chapter the main concepts included in the thesis are summarized and clarified. These include a brief explanation of the Standard Model and its interactions, basic principles and variables of proton-proton collisions, some ideas about charged-particle multiplicity and a review of dielectron, its sources within the collision and the signal extraction methods.

2.1 The Standard Model

Nowadays, the Standard Model is the physical model most widely accepted by the scientific community, since is the most accurate in describing the very basic components that makes up matter and the interactions between them. It was developed throughout the 20th century, by means of the difficult task of unifying the two key theories of the time: Quantum Mechanics and Special Relativity. This is how the Quantum Field Theories (QFTs) used by this model came about. Decades of mathematical development and a multitude of experimental verifications have shaped the current model. It is worth mentioning that the unification of these two theories mentioned above has not been satisfactorily resolved.

QFTs are based on the idea that for each type of particle there is an associated field $\phi(x)$. These fields are functions that depend on the space-time coordinates $x^\mu = (x^0, x^1, x^2, x^3) = (t, x, y, z)$. From here arises the covariant nature that the mathematical formulation of the theory must have. In turn, the evolution of these fields is marked by a lagrangian density $\mathcal{L}$, which must be invariant under Lorentz transformations. The equations of motion or evolution of the fields can be obtained using the Euler-Lagrange equations [3]

$$\frac{\partial \mathcal{L}}{\partial \phi_r} - \frac{\partial}{\partial x^\alpha}\left(\frac{\partial \mathcal{L}}{\partial \phi_{r,\alpha}}\right) = 0; \quad \begin{matrix} r = 1, ..., N \\ \alpha = 0, 1, 2, 3 \end{matrix} \tag{1}$$

with N the number of fields.

The first approaches to these QFTs arose around 1930 by physicists such as Dirac, Heisenberg, Pauli and Jordan, who eventually abandoned them because of their complexity and became detractors. It took twenty years for the fathers of the first QFT, Quantum Electrodynamics (QED), to solve the difficulties: Feynman, Schwinger and

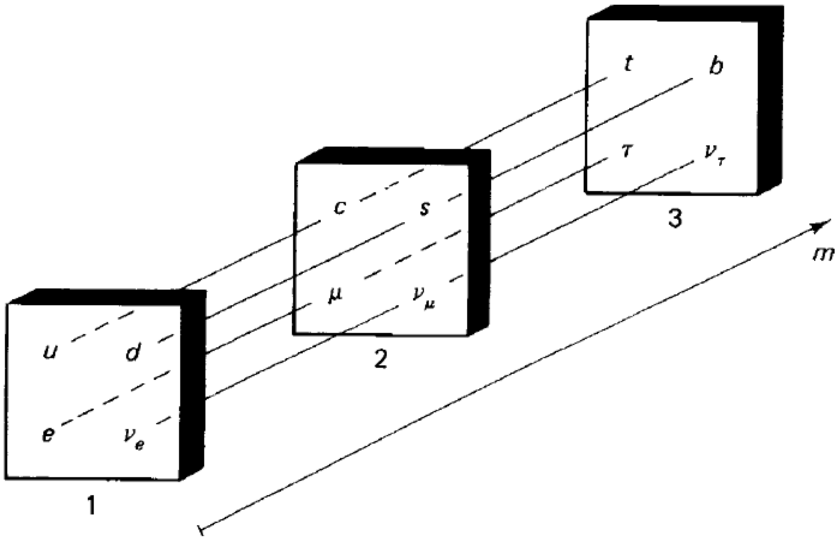

Figure 1: The three generations of leptons and quarks, in order of increasing mass. Taken from [4]

Tomonaga. Another fifteen or twenty years went by until the first electroweak theory appeared thanks to Weinberg, to unify the electromagnetic and weak interactions. It was also in the 1960s when Gell-Mann, among others, proposed the existence of quarks, whose subsequent development would form Quantum Chromodynamics (QCD). All these theories together compose the Standard Model as we know it today.

The Standard Model is based on three pillars:

- All matter is formed by elementary particles, which are classified into two types of subatomic particles within three families or generations [4]: the leptons, formed by the electron (e), the muon (μ) and the tauon (τ) together with their respective neutrinos (ν_e, ν_μ and ν_τ); and the quarks, grouped in up - down ($u-d$), strange - charm ($s-c$) and bottom or beauty - top ($b-t$). Each quark can come with one out of three colors (R, G and B) [5]. Of course, the presence of these particles implies the existence of the corresponding antiparticle, characterized by the same quantum numbers but with the opposite sign. This classification into families arises from the masses of the particles, coinciding with the chronological order of their experimental detection (see Fig. 1). All these elementary particles are fermions.

- The particles mentioned above do not live in isolation from each other, but rather there are interactions between them, giving rise to the physical effects we can detect and measure. These interactions are the electromagnetic force, the weak force and the strong force. For the moment, the gravitational force has had to be excluded of the model.

- Every time an interaction of this kind takes place is due to the exchange of a certain particle, which we call force carrier or intermediate particle. This mediators are the photon (γ) for the electromagnetic force, the $W^{\pm}$ and Z^0 bosons for the weak force and the eight gluons (g) for the strong force [1]. Mathematically, all these concepts are described through internal symmetries and group theory. To these mediators we must add the Higgs boson (H), which is responsible for the rest of the particles in the model having mass [7].

In Fig. 2 are summarized the main properties of the particles mentioned above.

The Standard Model is still considered a "model" instead of a "theory" due to the excessively large number of parameters to be determined from the experimental data. These are the masses of the lepton and quarks (that are 9), the gauge coupling constants of the Electroweak Theory and Quantum Chromodynamics (3), the CKM matrix parameters (4) and the masses of the $W^{\pm}$ and Higgs bosons (2): 18 in total [2]. Furthermore, certain sectors are of the opinion that the number of elementary particles is too large, and that some of them could be formed by combinations of the others, or that there is even a lower level in the scale of matter. In spite of this, and of some other problems that it has not been able to solve yet, it is the best framework we have to describe the Universe, both because of the surprising and numerous theoretical predictions and because of the precision of the experimental verifications.

[1] The boson behind the gravitational interaction would be the graviton G, but its existence has not been yet proven [6].

[2] And this is considering that neutrinos has no mass, which has been proven wrong in several experiments, adding 7 more free parameters [8].

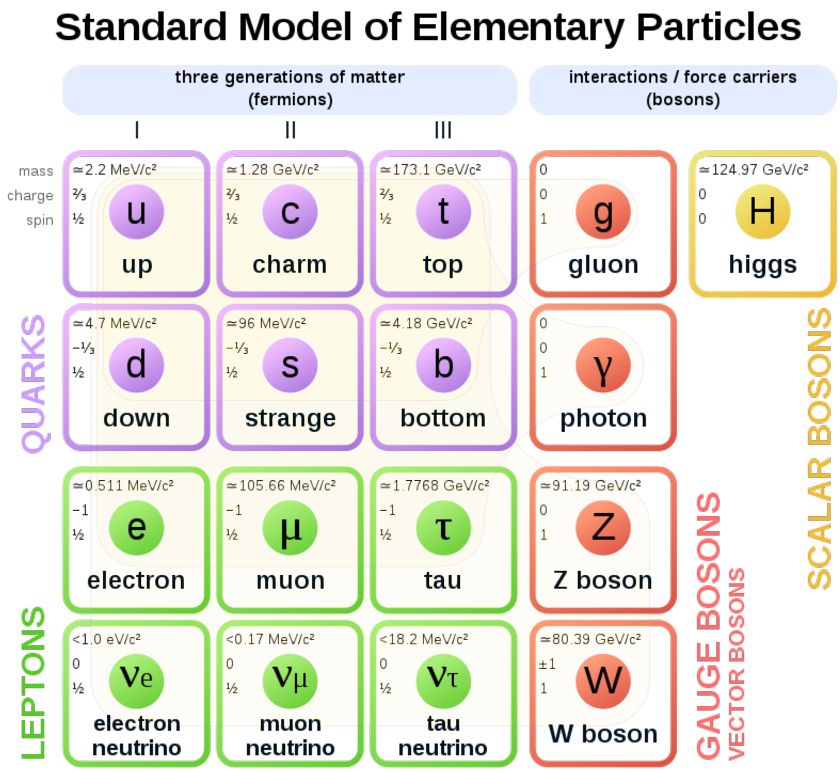

Figure 2: Fermions and bosons included in the Standard Model. Taken from [9]

2.1.1 Quantum Electrodynamics

QED was the first successful Quantum Field Theory. It was capable of describing the interaction between electrically charged particles, which took place through the exchange of photons (quanta of the electromagnetic field). One of the major advantages of this theory is that the classical form of the interaction was known, so that it could be taken as a starting point and adapted to the language of Quantum Mechanics and Relativity. And the opposite: there was a way to check the results obtained when facing the problem by other ways like gauge theories. This was crucial when studying the other two interactions, since they cannot be addressed by classical physics.

The strength of this interaction is characterised by the factor [10]

$$\alpha \equiv \frac{e^2}{4\pi\epsilon_0} \approx \frac{1}{137}, \tag{2}$$

where e is the charge of the electron and ϵ_0 is the permittivity in vacuum, and is called the fine structure constant. Is a dimensionless quantity, and because is such a small number it allows the application of perturbative calculations.

Using Heisenberg's uncertainty principle is easy to prove [11] that the range of an interaction is

$$R \leq \frac{1}{M_X}, \tag{3}$$

where M_X is the mass of the mediating particle. From here is immediate to verify that the electromagnetic force has an infinite range, as the photon is a massless particle.

2.1.2 Weak interaction

As we already said, the weak force (as well as the strong force) has no classical equivalent, so the way to clear the unknowns of this force was much more arduous. Unlike the electromagnetic force, the bosons responsible of the weak force do have mass, and not a small one: about 80 GeV for the $W^{\pm}$ and 91 GeV for the Z^0 [3]. Therefore, according to equation (3) their range is going to be very small, about 2×10^{-3} fm. The first hints of a new interaction in nature emerged when studying the β radiation, with the observation that electrons were emitted as a continuum of energies. Pauli suggested that an additional particle was emitted besides the electron [12], which would later be confirmed as the neutrino.

One of the most surprising aspects of this force is the fact that it does not conserve the discrete symmetries of P and C. This was experimentally confirmed by Wu in 1957 [13]. There were many problems completing the weak theory, until the discovery that it had to be coupled to the electromagnetic force, thus the electroweak theory emerged. The development of this theory also led to the Higgs mechanism of spontaneous symmetry breaking and the proposal of the existence of the Higgs boson. The presence of this particle has also been confirmed experimentally [14].

2.1.3 Quantum Chromodynamics

The Standard Model states that hadrons are formed by quarks, three for baryons and two (quark-antiquark pair) for mesons, and that the mediator of the strong interaction between two quarks is the gluon. This electric-neutral particle has no mass but does carry color charge. Therefore, like quarks, it cannot exist as an isolated particle. In the same way, hadrons must be formed in such a way that they are colorless particles. This is what is known as confinement, a concept which is still not very well understood today. The concept of color was introduced into the theory to explain the apparent violation of the Pauli exclusion principle by quarks. The strong interaction that occurs between hadrons is a reflection or a residue of the interactions between the quarks that form them. Indirectly, is the force responsible for protons and neutrons coming together to form nuclei. During a strong process the color of the quarks may change, but not their flavour.

Experimentally it was observed that, unlike with QED, the coupling constant in this processes α_s was greater than 1 [4]. As a consequence, the perturbative calculations seemed to be useless. However, one of the greater triumphs of QCD was the discovery that the value of α_s actually depended on the distance between the interacting particles. When this distance is relatively small (on the order of the size of a proton and smaller) α_s decreases substantially; this is known as asymptotic freedom. This means that inside a proton or some other similar particle the quarks can move without interacting much with each other. As the distance increases, the strength of the interaction becomes greater and greater, and the quarks attract more intensely. Because of this, and the confinement, strong interaction is only observed at small distances, even when the mass of the gluon is zero. It can be found that the coupling constant has the form [11]

$$\alpha_s(\mu) = \alpha_s(\mu_0)\left[1 + \frac{33 - 2N_f}{6\pi}\alpha_s(\mu_0)\ln(\mu/\mu_0)\right]^{-1}, \quad \mu^2 >> 1\ \mathrm{GeV}^2; \tag{4}$$

where μ is the difference between the squares of the momentum and energy exchanged $\mu^2 \equiv |\mathbf{q}^2 - E_q^2|$, N_f the number of quark flavours and $\alpha_s(\mu_0)$ the value of the constant at a reference value, usually at $\mu_0 = M_Z$ the mass of Z^0. This value is approximately $\alpha_s(\mu_0) = 0.118 \pm 0.002$. In Fig. 3 we can see the shape of α_s extracted from different experiments and compared to theoretical calculations.

At small distances (large transferred momentum), perturbative techniques (pQCD) can be employed. However, at large distances this is not possible. That is the reason why in those cases a technique called lattice QCD (lQCD) is used, in which spacetime is split into a lattice of discrete points and numerical calculations are made on that lattice. The number of points is then tended to infinity to obtain approximate results. The behaviour of the quarks can be simulated with a potential in the following way: at short distances,

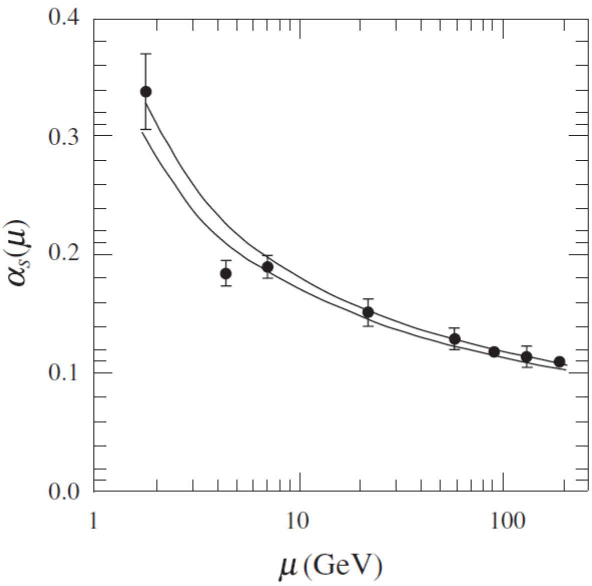

Figure 3: Shape of the strong coupling constant as a function of μ. Good agreement is observed between experimental data and the theoretical predictions. Taken from [11].

the exchange of one gluon predominates and it would have a Coulomb form; at longer distances, other processes would dominate and the potential would be approximately linear, so it would take the form

$$V(r) \approx -\frac{4}{3}\frac{\alpha_s}{r} + \kappa r. \tag{5}$$

It is a simple way of representing the potential between a quark and an antiquark. Spectroscopy experiments and then some lattice calculations have set the value of κ around 1 GeV/fm [15].

2.2 Proton-proton collisions

A major part of experimental physics focused on the investigation of subatomic particles is based on collisions. Through accelerators, beams of particles with a high energy (currently reaching a few TeV) are directed towards a target, that can be another particle approaching in the opposite direction, called colliding-beam experiment, or a fixed target, which can be formed by a wide variety of elements. The objective is to check how the particles of both the beam and the target behave when they collide with each other by the use of detectors. At sufficiently high energies a large number of new particles will form, whose properties are also studied.

The advantage of using fixed targets is that their composition can be prepared in advance. They can be made up of any minimally stable element. However, the energies that are achieved are lower, since work is done in the center-of-mass frame and part of the energy is used as kinetic energy of the target, so the energy available for the creation of particles is lower. When two particles travelling in opposite directions collide technically all the energy is available for this purpose, since the energy in this frame would be just [11]

$$E_{CM} = 2E_L, \tag{6}$$

being E_L the energy of the beams. Of course, this working method also has its disadvantages: the particles must be quite stable, and we must know how to produce them in the laboratory with the required energy, as well as being able to direct them towards the coming particle. The most commonly beams used are protons and electrons, as well as atomic nuclei.

2.2.1 Kinematic variables

There are a set of quantities that, because of their utility and interest, are always used in particle collision experiments. In relativistic terms, a particle with energy E, rest mass m_0 and momentum $\mathbf{p}$ is described by its four-momentum [16]

$$P = (E, \mathbf{p}) = (E, p_x, p_y, p_z). \tag{7}$$

In the accelerator the z-axis is often defined as the beam axis. Taking this into account, the momentum of the particle can be divided into longitudinal and transverse momentum

$$p_{\mathrm{L}} = p\cos\theta = p_z, \tag{8}$$

$$p_\perp = p\sin\theta = \sqrt{p_x^2 + p_y^2}, \tag{9}$$

with θ the polar angle or angle with the direction of the beam. $p_\perp$ is invariant under Lorentz transformations in direction z, but p_{L} is not invariant [17]. $p_\perp$ gives a rate of new created particles, since is new momentum arising in the perpendicular direction to the beam. We can also define the transverse mass as

$$m_\perp^2 = m_0^2 + p_\perp^2. \tag{10}$$

In a system of particles, the invariant mass m is obtained as [11]

$$m^2 = E^2 - \mathbf{p}^2, \tag{11}$$

being E and $\mathbf{p}$ the total energy and momentum. It has the same value in every reference frame. Is easier to evaluate in the CM-frame since $\mathbf{p}^2_{\mathrm{CM}} = \mathbf{0}$. For a single particle the invariant mass and the rest mass are the same.

In $2 \to 2$ processes are widely used the so-called Mandelstam variables:

$$s = (P_1 + P_2)^2 = (P_3 + P_4)^2, \tag{12}$$

$$t = (P_1 - P_2)^2 = (P_3 - P_4)^2, \tag{13}$$

$$u = (P_1 - P_4)^2 = (P_2 - P_3)^2, \tag{14}$$

where P_1 and P_2 are the four-momenta of the incident particles and P_3 and P_4 the four-momenta of the outgoing ones. This way, $\sqrt{s}$ is the energy in the CM-frame and $\sqrt{t}$ is the momentum transfer.

Velocity is not an additive quantity under several Lorentz transformations, so a new variable is defined, called the rapidity y. It can be expressed as [18]

$$y = \operatorname{arctanh} \beta = \frac{1}{2} \ln \left(\frac{1 + p_z}{1 - p_z} \right), \tag{15}$$

with[3] $\beta = v/c$. Is a dimensionless quantity and it can be positive or negative. At high-relativistic regimes, $y \cong 0$ if the particle is detected perpendicularly to the beam axis and $y \to \pm\infty$ if is detected in the same direction. Under a Lorentz transformation parallel to the beam axis we obtain [19]

$$y' = y - \operatorname{arctanh} \beta. \tag{16}$$

Thereby, when two particles are detected, the difference between their rapidities are indeed invariant:

$$y_1' - y_2' = y_1 - y_2. \tag{17}$$

Sometimes y can be difficult to determine, because one needs the energy and the polar angle of the particle, and we do not always have both. In those cases there is an alternative: the pseudorapidity η [20]. For ultra-relativistic particles it can be showed that [19]

$$y \approx -\ln \tan \frac{\theta}{2} = \eta. \tag{18}$$

[3]Here we have written c explicitly for clarity

2.2.2 Fundamental concepts in hadron-hadron collisions

Before the discovery of quarks, when studying electron-proton and proton-proton collisions it was noticed that proton was made of smaller charged particles inside of it [4]. This entities were called partons, forming the first model capable to explain the experimental data of collisions involving protons: the parton model. This model, in which multiple simplifications are made, starts from the idea that partons are the basic constituents of hadrons. They are fixed for each hadron, but there is also a cloud of partons constantly being emitted and absorbed called sea quarks. So that the hadron is not modified, since partons do not affect its quantum numbers, this fluctuations inside of it must take place in an lower energy scale Q^2 than that which the confinement occurs [22]. In the model is also considered that the momentum of this partons is almost colinear with the momentum of the proton [11]. Each one will carry a fraction x of the total momentum available. This way we can form what we call the Parton Distribution Functions (PDFs) $f_i(x, Q^2)$, that gives the probability of a parton of type i (quark, gluon or sea quark) carrying a fraction x of the momentum at the scale Q^2 [23]. Beforehand pQCD cannot be used to obtain the PDFs because of the energetic scales involved, so they have to be deduced from experimental data [24]. By convolution of parton cross sections with PDFs one can get hadron collisions cross sections.

The most common shape presented by PDFs is the one we see in Fig. 4. At small energy scales (left) we can see how the proton structure is given basically by the valence quarks (two u and one d), and that the contribution of virtual partons is small. One can appreciate that the sea quarks appear at low x because gluons with large momentum are suppressed by the form of gluon propagator [24]. On the other hand, at higher Q^2 (right) fluctuations grow and we observe a larger contribution of sea quarks and gluons for small x, and the role of valence quarks is less and less important.

At typical LHC energies the total hadron-hadron cross section is around 100 mb [22]. According to the way in which the interaction takes place we can classify the processes between hadrons (where naturally we include p-p processes) in the following ones:

- Elastic scattering: $hh \to hh$ (see Fig. 5 left).
- Single diffractive: $hh \to h + X + gap$, with X any new species not present in the

[4] More precisely, they were detected for the first time in deep inelastic electron scattering [21].

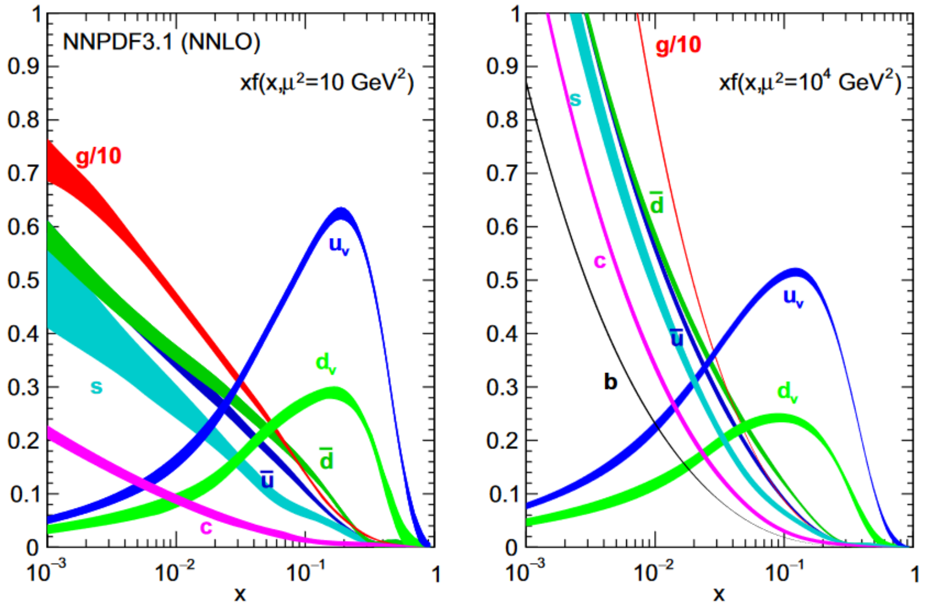

Figure 4: Examples of several Parton Distribution Functions for two values of the momentum transfer Q^2: 10 GeV^2 (left) and 10^4 GeV^2 (right). Taken from [25]

original beam and *gap* an empty rapidity region between the two of them (Fig. 5 center). In a process like this, one of the beams is excited and then it decays in a set of products that can be later detected.

- Double diffractive: $hh \to X_1 + X_2 + gap$. In this case both beams have broken up (Fig. 5 right).

To the diffractive processes one could also add multi-gap processes, e. g. central diffractive [26]. Depending on their transverse momentum, particles produced in a collision can be classified into two groups [17]: hard particles, when the moment is very high (they come from processes with $Q^2 > 2$ GeV^2), or soft particles, when $p_\perp$ is low. With the first ones pQCD can be applied, but not with the latter.

Inelastic and diffractive cross sections in p-p collisions are one of the basic observables when studying Particle Physics, so that they are always of great interest for the community. To study this hadronic cross sections are usually used concepts from Regge theory [27]. In this theory diffractive processes take place through the exchange of Pomerons, which are defined as singlet color objects with the quantum numbers of the vacuum (rep-

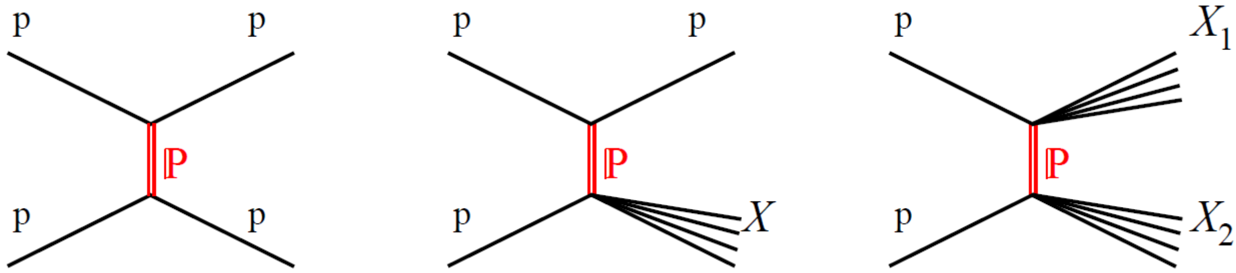

Figure 5: Elastic, single diffractive and double diffractive processes between two protons. A Pomeron is being exchanged. Taken from [27]

resented as a $\mathbb{P}$ in Fig. 5). The total cross section would be the sum of all cross sections of the processes mentioned above.

If in the collision hard parton-parton interactions have occurred we can define also underlying events (UE) or processes with low momentum transfer (therefore pQCD will not be useful either [22]). These are the remains of a scattering interaction like beam remnants, parton shower or hadronization. We will discuss them in Chapter 4.

2.3 Charged-particle multiplicity

The charged-particle multiplicity is defined as the number of charged particles produced in one event. Despite its simplicity and the fact that is a very simple quantity to measure in the laboratory it is a very useful tool. This is due the probability of producing n charged particles $P(n)$ in the final state is closely related to their production mechanism [28]. This function is called multiplicity distribution. However, from a theoretical point of view, it is very challenging to determine because of the lower scales of energies usually involved in this processes. When $P(n)$ follows a Poisson-like distribution it means that there are no correlations between the particles (the production of a new particle is independent of the already created ones). Any deviation from this behaviour suggests the presence of correlations.

There have been several attempts to deduce an analytical form that describes the multiplicity distributions at different energies $\sqrt{s}$. One of the first ones was Feynman, who started with the idea that the mean number of any kind of particle grows as [29]

$$\langle N \rangle \propto \ln W \propto \ln \sqrt{s}, \quad W = \sqrt{s}/2. \tag{19}$$

Through phenomenological arguments he concluded that the probability function of finding a particle i depended on the function $f_i(p_\perp, x = p_\mathrm{L}/W)$. Feynman's hypothesis claims that f_i does not depend on W at high energies, what is known as Feynman scaling.

Considering that the maximum possible y at a collision also grows as $\ln \sqrt{s}$ it is concluded that

$$\frac{\mathrm{d}N}{\mathrm{d}y} = \text{const.} \tag{20}$$

Consequently,

$$\left.\frac{\mathrm{d}N}{\mathrm{d}\eta}\right|_{\eta=0} \approx \text{const.} \tag{21}$$

Koba-Nielsen-Olesen scaling (KNO) was proposed in 1972 and is based on Feynman scaling, but taking into account the correlations. In this case, it can be shown that $P(n)$ scales as [30]

$$P(n) = \frac{1}{\langle n \rangle} \Psi \left(\frac{n}{\langle n \rangle} := z \right) + \mathcal{O} \left(\frac{1}{\langle n \rangle^2} \right), \tag{22}$$

where $\Psi(z)$ is a function independent of the energy. As a consequence every multiplicity distribution plotted as a function of z will fall into the same curve. This result as been noted as an approximation [31], so in reality $P(n)$ does not follow a universal function.

Another possibility is the use of the Negative Binomial Distribution (NBD)

$$P_{p,k}^{\mathrm{NBD}}(n) = \begin{pmatrix} n+k-1 \\ n \end{pmatrix} (1-p)^n p^k, \tag{23}$$

which gives the probability for having k successes after n failures in a Bernuilli experiment with a success probability of p [32]. So that one can apply this to the multiplicity distribution the relation between p and $\langle n \rangle$ has to be taken into account, getting to [33]

$$P_{\langle n \rangle,k}^{\mathrm{NBD}}(n) = \begin{pmatrix} n+k-1 \\ n \end{pmatrix} \left(\frac{\langle n \rangle / k}{1 + \langle n \rangle / k} \right)^n \frac{1}{(1 + \langle n \rangle / k)^k}. \tag{24}$$

The physical origin of this shape of the multiplicity distribution has yet to be understood. With a couple of simple assumptions, if we consider $k-1$ the fraction of the already present n particles stimulating emission of additional ones we can see that

1. k increases if the η-interval considered is enlarged;

2. k decreases with increasing $\sqrt{s}$ for a fixed η-interval.

Multiplicity distributions at high energies have been successfully fitted with a combination of two [5] NBD-shaped components: one for soft events and one for semi-hard events [34]. A fit with experimental data shows that the soft components follows KNO scaling and the semi-hard violate it.

At the actual LHC energies, multiplicity distributions are modeled according to QCD inspired models, considering that multi-parton interactions are going to rule the shape of this distributions. With different models from Monte Carlo event generators a good agreement between the experimental data and the predictions can be achieved, as we can see in Fig. 6.

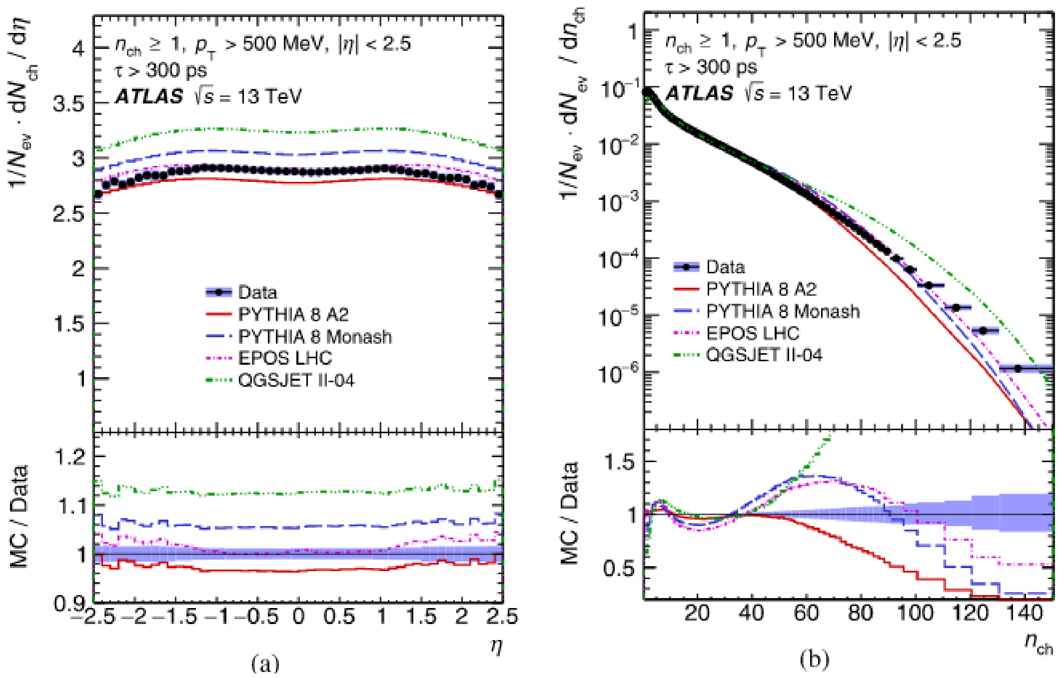

Figure 6: Primary-charged-particle multiplicity as a function of η (a) and multiplicity distribution (b). The bottom panels show the ratio between the experimental data and the predictions from MC simulations. Taken from [35]

[5] Sometimes more than two.

2.4 Dielectrons

As we already know, electrons are not sensitive to strong interaction. This is the reason why they are widely used in the study of high-energy ion collisions, as they can escape from the QGP medium without hardly any interactions, so they carry information about it at the moment of their creation [36]. Furthermore, electron-positron pairs are produced in every stage of the collision, so they also offer the possibility of showing the whole evolution of the system.

In multiple investigations (PHENIX and STAR Collaborations at $\sqrt{s}$ = 200 GeV [37–39], ALICE at $\sqrt{s} = 7$ and 13 TeV [1, 40]) the dielectron production in p-p collisions is well described by a cocktail of known hadronic sources. According to the invariant mass of the dielectron they proceed from one type of process or another. In the low mass region ($m_{\mathrm{ee}} < 1.1$ GeV) the dielectrons come from the two-body decay of a vector meson like $\rho(770)^0$, $\omega(782)$ and $\phi(1020)$. In addition, we can also find contributions from Dalitz decays of pseudoscalar and vector mesons:

$$\begin{gathered}\pi^0 \rightarrow e^+e^-\gamma \qquad \eta \rightarrow e^+e^-\gamma \\ \phi \rightarrow e^+e^-\eta \qquad \phi \rightarrow e^+e^-\pi^0 \\ \omega \rightarrow e^+e^-\gamma\end{gathered}$$

Matter in fact the process $\pi^0 \rightarrow e^+e^-\gamma$ will be the most prominent. In Fig. 7 we can see the Feynman diagram of these two processes. In the direct decay of a vector meson (right) the intermediate of the process is a photon; in a Dalitz decay, in addition to the dielectron pair, a photon or a pseudoscalar meson is produced (center and left). All this particles are light mesons, because they only contain u, d or s quarks.

In the intermediate region ($1.1 < m_{\mathrm{ee}} < 2.7$ GeV) the main contribution is the semileptonic decay of charm and beauty hadrons. This electrons are correlated as follows: at early stages of the collision a heavy quark-antiquark pair (c or b) is created, to preserve flavour conservation. Each one will form an open charm (D) or beauty (B) meson, which in turn will decay through the semileptonic way. Then this electrons are detected at the same time, resulting into a dielectron. These processes give rise to a continuum at intermediate masses. Thanks to these dielectrons it is possible to extract the initial kinematic relation between the original quark and antiquark, although in the case of beauty b is

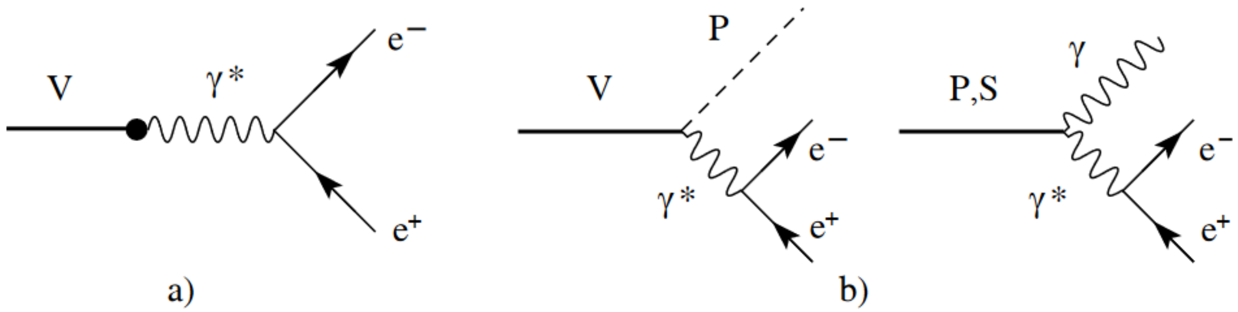

Figure 7: Feynman diagrams of the decay of the particles that contribute to the dielectron spectrum: a) a vector meson (V) decay in dielectron through a photon; b) diagrams of the two types of Dalitz decay, in which a vector meson decays into a dielectron and a pseudoscalar (P) meson or a pseudoscalar or a scalar (S) meson decay into a photon and a dielectron. Taken from [41]

very weakened due to the large mass of the quark. The branching ratio of a semileptonic decay of a D meson is about 10% [42]. As we go up in the mass range the number of events is usually lower, so there will be more statistical uncertainty.

At higher masses ($3 < m_{\text{ee}} < 4$ GeV) one expects the contributions from two-body and Dalitz decays of charmonium J/ψ and its radial excitation $\psi(2S)$.

In Fig. 8 the results from a p-p collision at $\sqrt{s} = 13$ TeV in the ALICE experiment are shown. On the left the dielectron cross section as a function of the invariant mass m_{ee} is plotted. The experimental data is compared to the hadron cocktail obtained in Monte Carlo simulations with PYTHIA, so the charm and beauty cross sections could be extracted. The data is in good agreement with what was expected from the previous calculations. On the right the cross section as a function of the transverse momentum $p_{\perp,\text{ee}}$ is shown for three different intervals of mass.

However, the main contribution that arise from the measurement is the so-called combinatorial background. This signal of the spectrum comes from electrons originated in different mother particles, mainly due because of the method followed to extract the signal (see subsection 2.4.1). Electrons from photon conversion are another significant source of background; these are electron-positron pairs that comes from a photon that has entered in the detector and has interacted with the surrounding materials. These pairs will appear with an apparent finite invariant mass, so they will affect the signal. Clearly all this

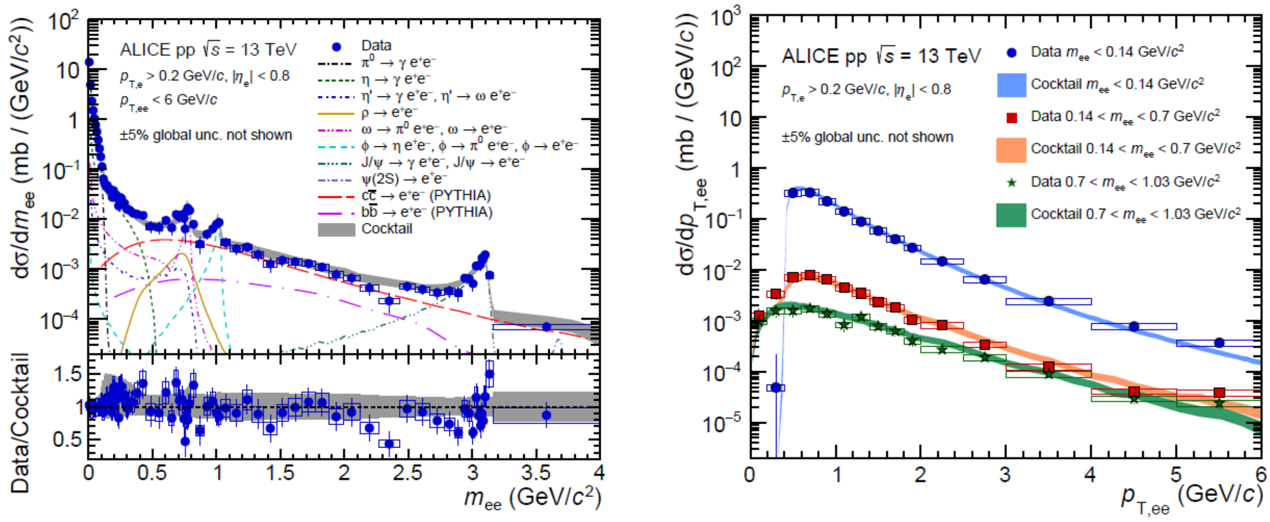

Figure 8: Dielectron cross sections as a function of the invariant mass (left) and the transverse momentum (right) for p-p collisions at $\sqrt{s} = 13$ TeV. The data is compared to the results of Monte Carlos simulations. At bottom left the ratio between the data and the expected values is shown, proving that they are in good agreement. Taken from [40].

background implies some trouble, and it has to be eliminated or, at least, minimized. In the next sub-section some techniques will be shown to do so.

The Fig. 9 provides a very visual description of all the electron sources contributing to the dielectron spectrum. The true signal is given by the processes showed at the top (decays from light mesons) and the bottom (correlated electrons from D and B mesons). In the center is shown the photon conversion process, which produce real pairs but are considered as background. Above all this processes the combinatorial background will appear, composed by pairs of electrons coming from different mother particles.

2.4.1 Measurement and data analysis

Even though in every experiment focused on the study of dielectrons the signal extraction methods are quite similar in this thesis were selected the techniques conducted in [40], but they are quite similar every time the dielectron signal is measured. The data was originally taken in the ALICE experiment (see Chapter 3) during the 2016 LHC pp run at $\sqrt{s} = 13$ TeV.

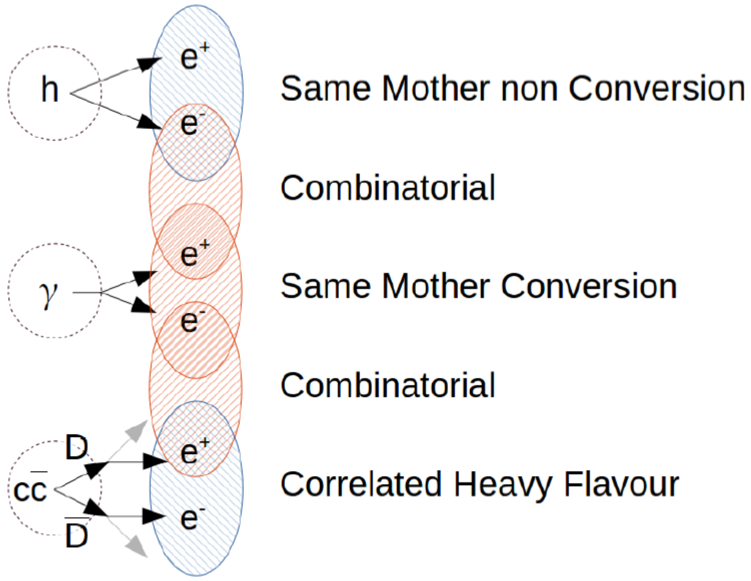

Figure 9: Processes that form the dielectron signal: decays of light hadrons (top), photon conversion (middle) and decays from heavy flavour mesons (bottom). The blue area forms the signal, and the red area, the background. Taken from [43]

The first step is to select only the electron candidates with $p_{\perp,\mathrm{e}} > 0.2$ GeV in the range $|\eta| < 0.8$. In a real situation one does not know the origin of each electron, so some statistical-based methods need to be applied to eliminate the background B and extract the actual signal S. All the selected electrons found in an event are paired to form dielectrons. By doing so opposite-sign pairs N_{+-} but also same-sign pairs N_{++} and N_{--} are obtained. Of course the latter are not part of the signal.

In fact, is assumed that these same-sign pairs in the same event can be used to estimate the combinatorial background through the geometric mean $\sqrt{N_{++}N_{--}}$. In addition, to adjust the different detector acceptance to opposite and same-sign pairs a correction factor R is inserted, with the form

$$R = \frac{M_{+-}}{2\sqrt{M_{++}M_{--}}}, \tag{25}$$

where M_{+-} and $M_{\pm\pm}$ are opposite-sign and same-sign pairs from mixed events, respectively. After doing all that, the signal is extracted according to the following equation:

$$S = N_{+-} - B = N_{+-} - 2R\sqrt{N_{++}N_{--}}. \tag{26}$$

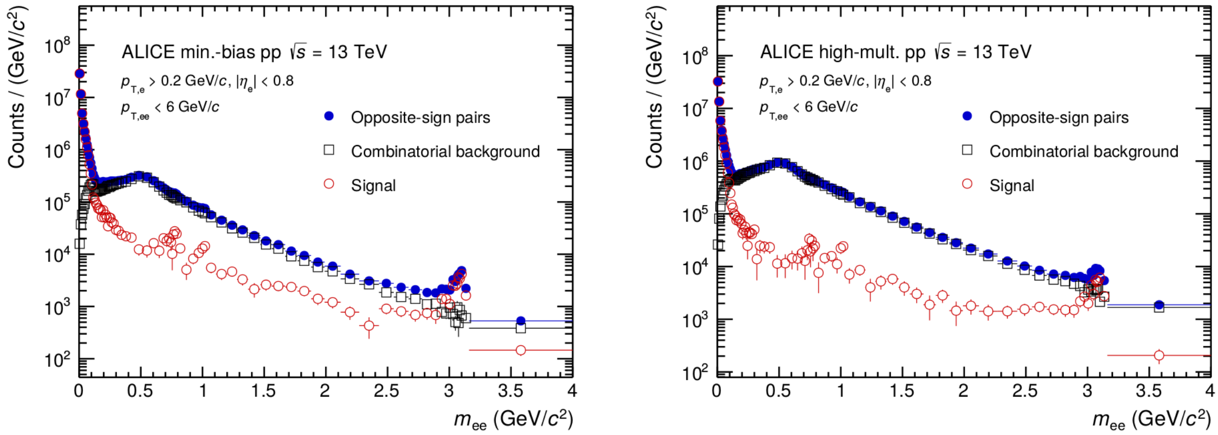

Figure 10: The spectra of opposite-sign pairs, combinatorial background and signal are shown for minimum bias (left) and high-multiplicity events (right). Taken from [40]

In Fig. 10 is shown the shape of this spectra, before subtracting the combinatorial background B and after doing so, for minimum-bias and high-multiplicity events..

In addition, dielectrons coming from photo conversion in the material of the detector will cause a lot of background in the lower mass region. To get rid of it, first they are selected by certain cuts and triggers on the different parts of the detector (see section 3.2), eliminating more than 93% of them. After that, the ones that passed the selection are removed using their orientation to a magnetic field in the detector. Less than 1% of those remaining will contribute to the final spectrum [1].

2.4.2 Hadronic cocktail

Experimental data is compared to the expected contribution from each hadron mother obtained by the use of a fast Monte Carlo simulation.

To get an approximation of the pion $p_\perp$-spectrum the charged-hadron spectrum was scaled by the pion-to-hadron ratio calculated in [1]. For the rest of the particles, it was made a fit of the ratios η/π^0, ρ/π^0 and ω/π^0 measured at p-p collisions with $\sqrt{s} = 2.76$ and $\sqrt{s} = 7$ TeV [44, 45]. For ϕ a scaling was also made but with $m_\perp$ this time, replacing $p_\perp$ with $\sqrt{m^2 - m_\pi^2 + p_\perp^2}$ [46]. This results were obtained with PYTHIA6 and PYTHIA8. The decays of this particles were originally simulated in [1] with the event generator EXODUS. The contribution from J/ψ was simulated with PYTHIA6.4 at $\sqrt{s} = 13$ TeV and was normalized to its cross section, extrapolated from measurements of $\sqrt{s} = 7$ TeV. The contribution from $\Psi(2S)$ was normalized from the J/ψ cross section. After doing all that a Monte Carlo simulation is conducted to obtain the detector response to these contributions.

To get the contributions from related semileptonic decays of charm and beauty mesons two event generator were used: Perugia 2011 tune for PYTHIA6.4 and POWHEG. Both have NLO (next-to-leading order) processes integrated. The two results obtained with the two of them are slightly different [40].

3 ALICE experiment

ALICE (A Large Ion Collider Experiment) is a detector located at the CERN complex, more precisely in the Large Hadron Collider (LHC). The main goal of this experiment is to study the quark-gluon plasma via ultra-relativistic heavy-ion collisions [47]. This plasma is formed when matter is subjected to a pressure and temperature so high that quarks and gluons can be found in a deconfined state, something impossible in the usual conditions we found matter. The main reason behind focusing on this is to understand better the strong interaction, since QCD predicts the existence of this plasma.

Its dimensions are $16\times16\times16$ m^3, and it features 18 different detector systems, each one designed for a specific purpose. It has been optimized to provide an excellent Particle Identification (PID) at the extremely high particle multiplicity present in the LHC. The major part of ALICE its the central barrel, formed by different concentric layers of detectors (see Fig. 11). These are the Inner Tracking System (ITS) with six planes of Silicon Pixel (SPD), Drift (SDD) and Strip (SSD) Detectors, the Time-Projection Chamber (TPC), three arrays of Time-of-Flight (TOF), Ring Imaging Cherenkov (HMPID) and Transition Radiation (TRD) detectors for PID, and two electromagnetic calorimeters (PHOS and EMCal). Several smaller detectors (ZDC, PMD, FMD, T0, V0) are distributed at small angles for global event characterization and triggering. For its relevance in dielectron detection we are going to focus on the ITS, TPC, V0 and TOF.

3.1 ALICE detectors and dielectron

3.1.1 Inner Tracking System

It has been optimized for particle identification and tracking of low-momentum particles (below 200 MeV). Another function is the improving of resolution for particles reconstructed by the TPC. It serves as a stand-alone particle spectrometer. Another essential capability of the ITS is the determination of the position of the primary interaction vertex and the identification of secondary vertices. This is crucial for the localization of related electrons.

The ITS consists of six cylindrical layers of three different silicon-based detectors. It covers the pseudorapidity range of $|\eta| < 0.9$ at radii between 3.9 and 43.0 cm. The nature

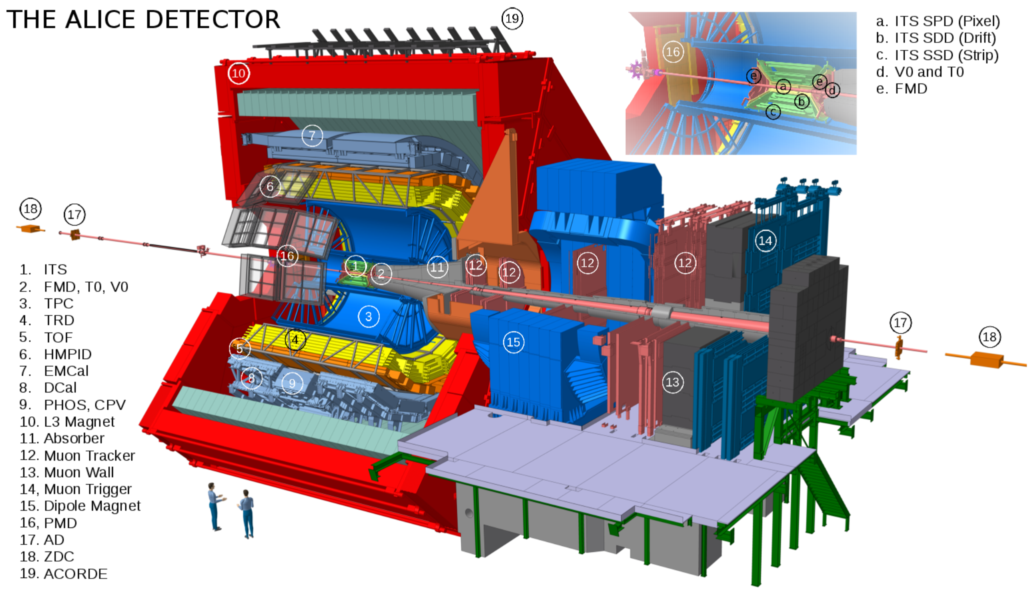

Figure 11: Schematic view of the ALICE experiment and its multitude of different detection systems. Taken from [48]

of the layers is the following:

- The first two layers are formed by Silicon Pixel Detectors (SPD). They are located at radii of 3.9 and 7.6 cm, covering a range of $|\eta| < 2$ and $|\eta| < 1.4$. It is made of 10 million hybrid silicon pixel cells with a dimensions of 50 μm in $r\phi$ direction and 425 μm in z direction.

- The next two layers are Silicon Drift Detectors. They are located at radii of 15 and 23.9 cm, covering both a range of $|\eta| < 0.9$.

- The two outer layers have Silicon Strip Detectors (SSD). They are located at radii of 38 and 43 cm, covering both a range of $|\eta| < 0.98$. These, and the two before, can be used for PID through energy loss signal $\mathrm{d}E/\mathrm{d}x$ in the non-relativistic region.

3.1.2 Time Projection Chamber

The TPC is a gas chamber-based detector, and the main tracking device. In addition, is also a particle identification detector in the region of the relativistic rise, up to momenta of about 50 GeV. It covers $|\eta| < 0.9$ for tracks with full radial track length. In the $p_\perp$ range, it covers from about 0.1 GeV to 100 GeV with good resolution. The detector is a cylinder with an inner radius of 85 cm and an outer radius of 250 cm for the active volume. The overall length along the z direction is 500 cm.

The active volume is filled with a gas mixture of Ar-CO_2. When a charged particle enters in the detector it ionizes the molecules of the gas. Thanks to a high voltage applied to the cylinder, the new electrons present travels toward the end of the chamber, carrying information about the energy of the particle with them. Because of the high number of pads distributed in the detector and the measurement of the arrival time of the electrons (which is translated into z coordinates) it counts with 557 million voxels to reconstruct three-dimensional tracks of the particles. This leads to the capacity of forming up to 159 spacial points per track.

The nature of each particle is determined from its mass, that can be obtained thanks to its energy loss $\mathrm{d}E/\mathrm{d}x$ and its momentum. The momentum can be determined with a constant magnetic field applied in the detector.

3.1.3 Time-of-Flight detector

This array is designed for large acceptance and average momenta. It measures the arrival time of particles relative to the event collision time. The area of coverage is about 140 m^2 with 160 000 individual cells at a radius close to 4 m. It covers the central pseudorapidity region for PID in the intermediate momentum range. Coupled with the ITS and TPC is capable of providing event-by-event identification of larges samples of pions, kaons and protons. It is also a gaseous detector.

The basic unit of the system is a 10-gap double-stack Multi-gap Resistive-Plate Chamber (MRPC) strip, which dimensions are 122×13 cm, with an active area of 120×7.4 cm^2. This area is in turn divided into two rows of 48 pads. The overall active region length is 741 cm.

3.1.4 V0 system

It is formed by the V0A and V0C detectors, which are two arrays of scintillator counters on either side of the ALICE interaction point. The V0 is used as minimum bias trigger and for rejection of beam-gas background. The triggers are given by particles coming from initial and secondary interactions. It can be used to determine the centrality of a collision via the measurement of the event multiplicity. The detector also contributes to the measurement of luminosity in proton-proton collisions.

The two arrays cover a range of $2.8 < \eta < 5.1$ for the V0A and $-3.7 < \eta < -1.7$ for the V0C. They are divided into 32 counters distributed in 4 rings.

3.2 Particle tracking and PID

We are going to briefly elaborate on the usual process followed for particle tracking and PID in ALICE, focusing on the dielectron detection.

The track determination process begins at the SPD, the innermost detector of ALICE. There, the primary vertex has to be located, from which the tracking of the particle continues through the TPC. To reconstruct the primary vertex a pair of points in the two layers of the SPD are taken, which must be close in azimuthal angle in the transverse plane. The resolution of their position depends on the charged-particle multiplicity of the track. The location of secondary vertices is conducted in further tracking analysis. It is very important to have high-resolution tracks to study particles with a very short mean life such as charm and beauty decays.

The electrons are selected enforcing basic criteria to the reconstructed tracks at the ITS and TPD, in addition to the kinematics constraints that one needs (in this case, $|\eta| < 0.8$ and $p_{\perp,\mathrm{e}} > 0.2$ GeV [40]). Tracks on the ITS must have hits in at least 5 out of 6 of the layers, and around 100 points out of 159 available on the TPC [1]. Requiring a maximum distance of closest approach (DCA) to the primary vertex and the transverse plane ($\mathrm{DCA}_{xy} < 1$ cm) and in longitudinal direction ($\mathrm{DCA}_z < 3$ cm) one manages to reduce the contribution of secondary tracks. To eliminate electrons from photon conversion is required that they have one hit in the first layer of the SPD.

To carry out the identification of charged particles the information provided by the ITS, TPC, TRD, TOF and HMPID is collected. Each one of these detectors will be optimal for its own specific momentum range. The best results are obtained combining the data of several detectors.

Like we have already said, the four outermost layers of the ITS are used for PID in a low-momentum range through the ionization energy loss $\mathrm{d}E/\mathrm{d}x$. The same applies to the TPC. When these detectors fail, in the region of minimum energy loss, the TOF comes into play to identify the particle. The energy loss depends at first order on the charge of the particle, its velocity β and Lorentz factor γ, and can be described with a Bethe-Bloch curve. This can be parametrized with a formula proposed by the ALLEPH collaboration [49]:

$$f(\beta\gamma) = \frac{P_1}{\beta^{P_4}} \left[P_2 - \beta^{P_4} - \ln\left(P_3 + \frac{1}{(\beta\gamma)^{P_5}} \right) \right], \tag{27}$$

with P_{1-5} some fit parameters. In Fig. 12 we can see the results of the measurement of $\mathrm{d}E/\mathrm{d}x$ as a function of the momentum, and the predicted Bethe-Bloch curve (black lines), for several different charged particles. In most regions the identification is quite easy, but in some of them we appreciate overlap of the different curves. In those cases more sophisticated methods have to be applied like Gaussian fitting to the energy loss.

To identify the electrons, the information mainly comes from the data provided by the TPC and the TOF. The way of expressing the response of a detector to PID is via the deviation of the expected and the measured ionization energy loss for a certain kind of particle i and momentum $n\left(\sigma_i^{\mathrm{DET}}\right)$, normalized by the detector resolution $\left(\sigma^{\mathrm{DET}}\right)$. Like that, one can select the electrons and reject other charged particles. In [40], electron are accepted if $\left|n\left(\sigma_i^{\mathrm{DET}}\right)\right| < 3$.

To further suppress the remaining conversion pairs another selection criteria is applied [1]: when the extrapolation of these tracks to the point of collision is made it appears a non-vanishing artificial opening angle between the electron and the positron with respect to the internal magnetic field of the detector. This angle will be situated in a plane perpendicular to the magnetic field with more preference, so with the right selection cut a large number of the remaining pairs can be removed.

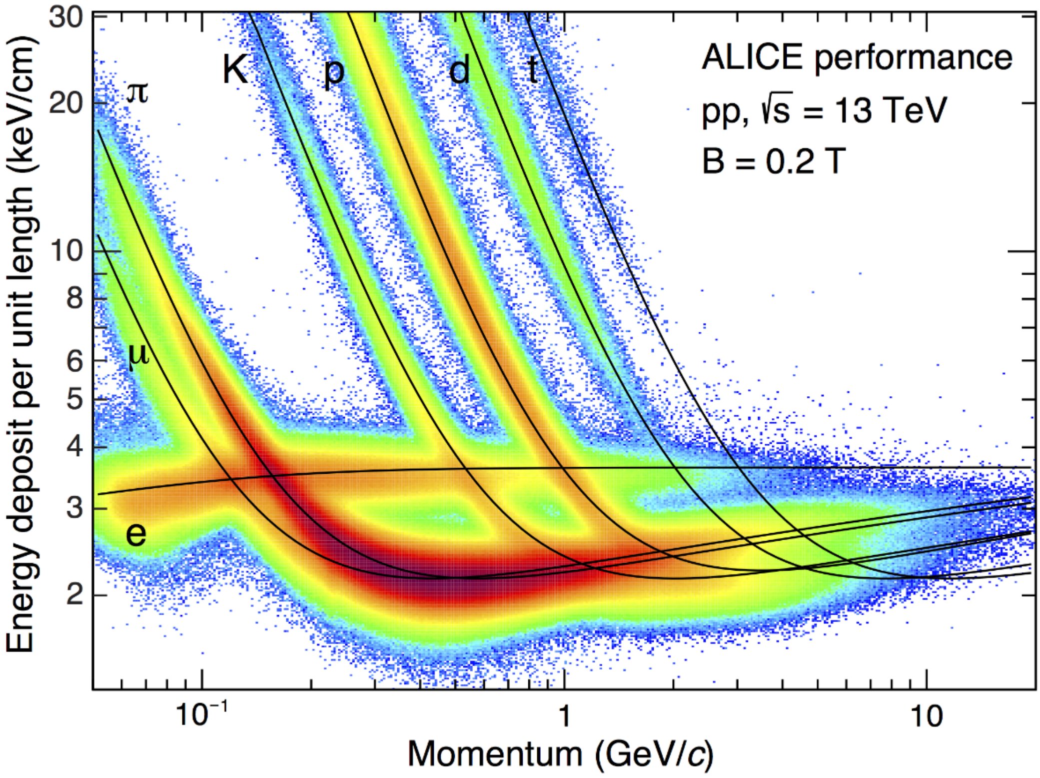

Figure 12: Experimental results of the ionization energy loss $\mathrm{d}E/\mathrm{d}x$ of different species of particles in the TPC. It is also shown the expected values from the Bethe-Bloch formula. Taken from [50]

4 PYTHIA8

PYTHIA is a Monte Carlo based event generator designed to simulate proton-proton collisions, mostly, but also lepton, proton-nucleus and nucleus-nucleus collisions, at high energies (CM energy must be greater than 10 GeV [51]). Thanks to its ability to simulate this variety of processes is a software widely used by the research community, being very useful for both theoretical and experimental work, mainly in LHC investigations. It has a very complex physics model implemented based on QCD theory, but also on experimental data through phenomenological models. Because of that, it can simulate a proton-proton collision with a multitude of several processes between the partons and all the new particles created in the collision. With this powerful tool we can simulate this high-energy collisions and look for the dielectrons. The outgoing particles created in the process are produced in the vacuum.

Here we see this schematic in Fig. 13 that represents a very simplified way of see how PYTHIA treats collisions, and even so one can appreciate how complex the proton

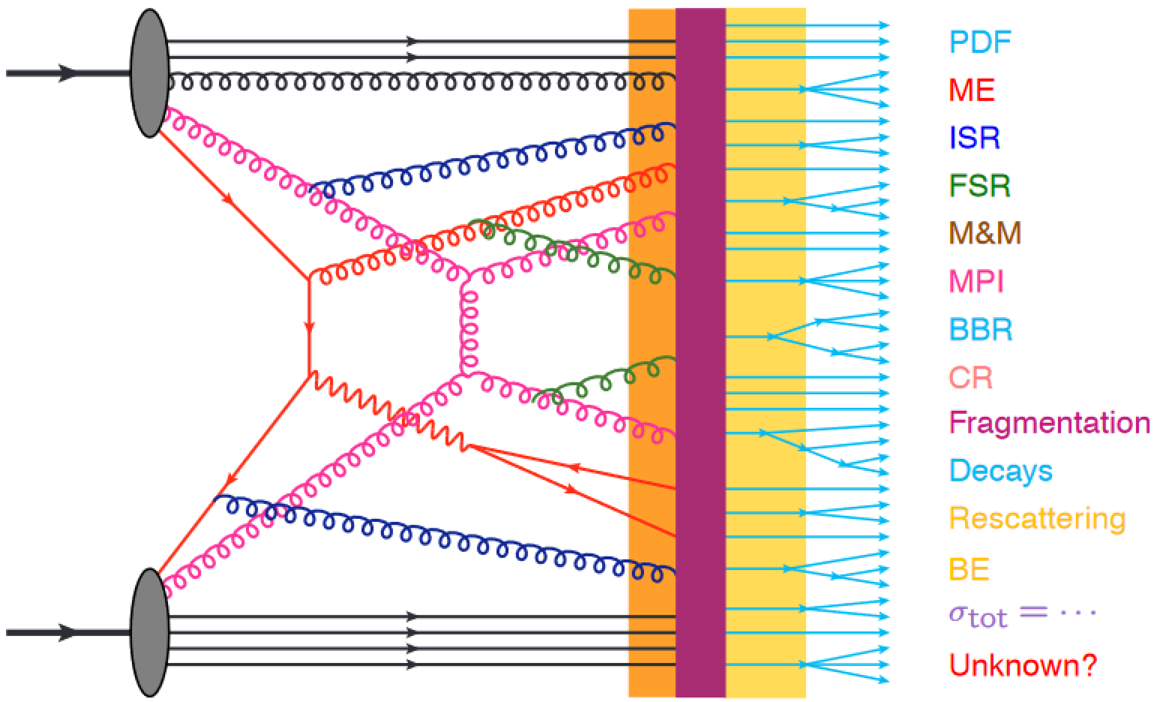

Figure 13: Schematic figure of a proton-proton collision in PYTHIA. Taken from [52]

collisions in the simulations are, and of course, in real life. The steps of the collision this figure depicts are the following ones:

- **Partonic scattering**. As a consequence of the fact that protons are not elementary particles and they are indeed made of partons (quarks, gluons and sea quarks) to describe the collision one must have into account this particles, that will be the ones interacting at high energies. PYTHIA is capable of include single but also multiple scattering between the partons. Perturbative QCD is assumed to describe the interactions, with the regularization of the cross section divergence when $p_T \to 0$ [53].

- **Parton shower**. In addition to the Multiparton Interactions (MPI), calculation of Initial State Radiation (ISR) and Final State Radiation (FSR) cross sections has to be implemented in the algorithms [51]. This is essential in order to predict what the final state of the system will be after a collision in an experiment, e. g., the LHC [54]. In the course of a process like this a gluon, for example, can split into heavy-flavour quark-antiquark pairs [26].

- **Beam remnants and color reconnection**. After all these interactions between the partons have taken place, it is possible that some other partons have been left behind, the ones that have not interact yet. They are called beam remnants. These partons are not part of the ISR or the FSR [55] and can be quite complicated sometimes. Also, to preserve flavour conservation, when a sea quark is torn away from the proton it must leave behind the correspondent antiquark in the beam remnant. We call this partons companion quarks [56]. In the unlikely event that no sea quarks need to be added because there is no valence quarks left in the hadron the beam remnant is represented as a gluon.

  As a consequence of these processes we will end up with a certain number of colored partons connected via the so-called strings, so that the whole system is colorless. However, the increase of the average transverse momentum as a function of the charged particle multiplicity present in data from the LHC could not be explain at first, so the color reconnection mechanism (CR) had to be introduced [57]. In order to fit the data, studies suggest that CR is produced in such a way that the string

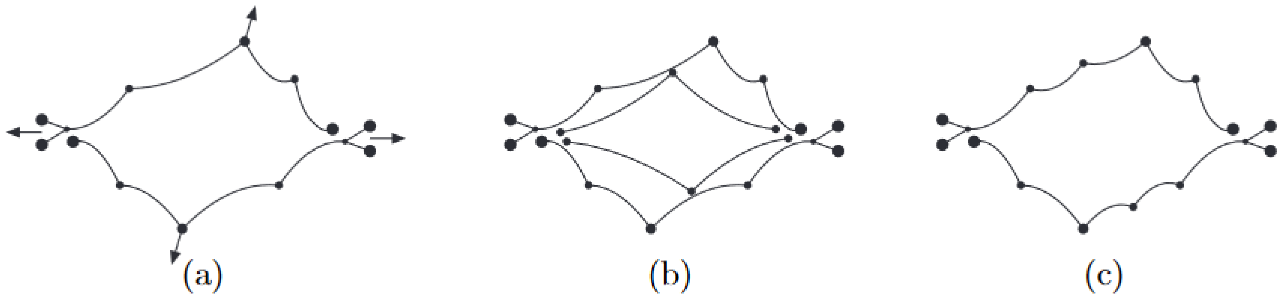

Figure 14: Mechanism of color reconnection (CR): (a) After a hard scattering process, the partons would end up connected via string. (b) Other steps of the collision like MPI and ISR would create more partons and their respective color string. (c) To fit the experimental data available, the strings have to be as short as possible. Figure taken from [59].

length is as short as possible [58]. In Fig. 14 we see how this process would be carried out. Currently there are three different CR models implemented in PYTHIA, each with its own method of reducing the string length [51].

- **Hadronization**. The di-quark states, i. e. quark-antiquark pairs that can be found in the system begin to move apart, so the string between them grows and the energy stored in it increases, until it breaks and forms a new quark-antiquark pair. If there is enough energy, the process will repeat itself until a new pair cannot be formed. This is the process in which new hadrons are created, or hadronization. The colored partons are transformed like that into color singlets or colorless particles. In PYTHIA this mechanism is implemented via the Lund model [60], that will be discussed below. Then, the new particles will decay (if it is the case) with their respective branching ratio.

From all this particles produced by PYTHIA we will select the electrons and positrons, and then pair them to form the dielectron we are looking for.

4.1 The Lund model

Let's go a little deeper into the physical model used by PYTHIA (and some other event generators [52]) to describe the hadronization process. This model is based on the fact that the confinement that occurs between a quark-antiquark pair can be described by a potential of the form like the eq. 5 [15]. The linear term will be the only one taken into account to describe the fragmentation and hadronization of the quark pairs.

If we consider the behaviour of a couple of massless particles (like a $q\bar{q}$ pair in this simplified case), its classical motion can be described with a Hamiltonian of the form [61]

$$H = T + V = |p_1| + |p_2| + \kappa |z_1 - z_2|, \tag{28}$$

where p_1 and p_2 are the momenta and z_1 and z_2 the positions of these particles. If one solves the Hamiltonian and calculates the equations of motion, considering that the particles move out along the z-axis, he will obtain

$$\left| \frac{\mathrm{d}p_{z,1/2}}{\mathrm{d}t} \right| = \left| \frac{\mathrm{d}p_{z,1/2}}{\mathrm{d}z} \right| = \kappa, \tag{29}$$

where the sign depends on where the particle is moving to. The motion of the system will then be like a "yo-yo", since as seen from the CM frame the particles move away and come together at regular intervals at the speed of light. We can see this in Fig. 15(a). As each quark usually emerge with a different energy, the most common way of seeing this is applying a boost, like we see in Fig. 15(b).

Assuming that the string is not going to break, we would see a simple harmonic motion, in which the quarks split with a certain amount of energy and separate for a period of time $t = E_{\mathrm{CM}}/2\kappa$. In that moment, all the energy has been transferred to the string, which pulls the quarks back to their starting position. When its length is zero (at $t = E_{\mathrm{CM}}/\kappa$), now are the quarks that have the energy again, so they start to move away in the opposite direction, and the process begin again. In present models it is consider the the string breaks so fast that it is enough to take into account only the first elongation [15].

When the invariant mass of the system is larger than the invariant mass of the quark-antiquark pair, then the string will break. The new pair $q'\bar{q}'$ will repeat the same process as the previous one, until the available energy is insufficient to create a new pair (Fig. 16). Generally, the evolution of each string is independent of the others, so the breaking

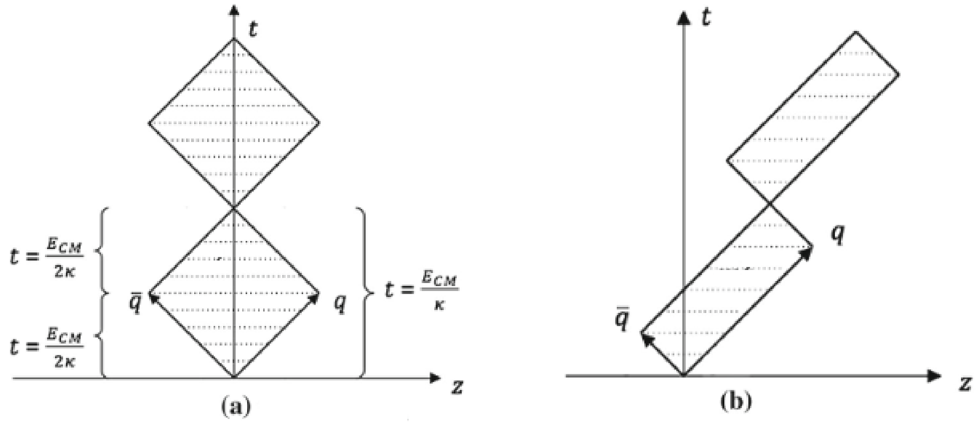

Figure 15: Motion of the massless-two-particle system in the CM frame (a) and after a boost (b). Adapted from [15].

can be described in the most convenient order [51]. In addition, during the whole process of pairs creation the color of the particles must be adequate for the entire system to be colorless.

But what happens if we consider that the particles are created with a certain mass and transverse momentum? Then they would appear like virtual particles. In that case, the Lund model takes ideas from the concept of quantum tunnelling [55]. According to Quantum Mechanics, the pair of quarks may be created at the same point in space to preserve local flavour conservation. But classically, they should be located at a certain distance so the string that joins them can get an amount of energy equivalent to their transverse mass $m_\perp$. Therefore, the quarks pass from the point of creation to the zone classically allowed via tunnelling, with a probability given by

$$\exp\left(-\frac{\pi m_\perp^2}{\kappa}\right) = \exp\left(-\frac{\pi m^2}{\kappa}\right)\exp\left(-\frac{\pi p_\perp^2}{\kappa}\right), \tag{30}$$

with the string tension $\kappa \approx 1$ GeV/fm ≈ 0.2 GeV^2. This leads to a suppression of the production of heavy quarks, with a ratio of [61]

$$u\bar{u} : d\bar{d} : s\bar{s} : c\bar{c} \approx 1 : 1 : 0.3 : 10^{-11}. \tag{31}$$

Therefore, strange and charm production can never occur during this soft process (it takes place in perturbative processes).

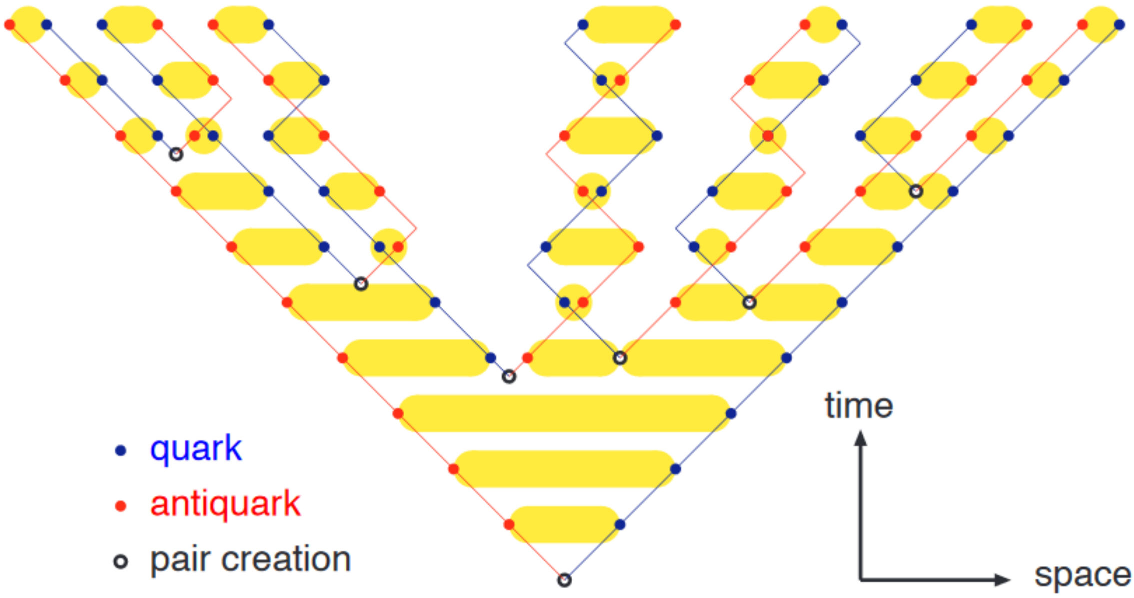

Figure 16: Schematic of how the iterative process of string breaking and pair creation leads to new hadrons. Taken from [52].

If we wanted to also include heavy quarks we would have to extend this model so simplified. Let us assume that we want to simulate the fragmentation process of a $c\bar{c}$ pair. In this case the particles would not move at the speed of light, so the trajectory described by them would be a hyperbola. Its asymptotes would be the straight lines formed by the motion of the massless particles, as we can see in Fig. 17. From the relativistic description of the force $\mathrm{d}p_z/\mathrm{d}t = \pm\kappa$, the equations of this new behaviour would be [15]

$$p_{z,c}(t) = p_0 - \kappa t, \tag{32}$$

$$E_c(t) = \sqrt{p_{z,c}^2(t) + m_c^2}, \tag{33}$$

$$z_c(t) = \frac{E_0 - E_c(t)}{\kappa}, \tag{34}$$

with $p_0 = p(t = 0)$ and $E_0 = E(t = 0)$. The antiparticle $\bar{c}$ would follow the mirror trajectory. The fragmentation process would be carried out the same way but taking into account the new motion curves.

The pair of quarks that has been created will dictate the flavour of the meson, but its nature has not been fully established. For this purpose, the program has six different

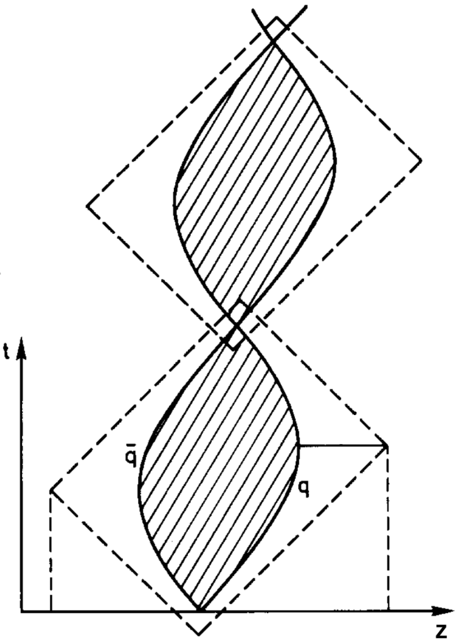

Figure 17: Motion of two massive particles in the CM frame. The asymptotes are the trajectories of the massless particles. Adapted from [61].

multiplets available, which will be selected depending of the spin of the quarks and certain simple rules of probability. The multiplets are [55]

- Pseudoscalar meson: $L = 0, S = 0, J = 0$
- Vector meson: $L = 0, S = 1, J = 1$
- Axial vector meson: $L = 1, S = 0, J = 1$
- Scalar meson: $L = 1, S = 1, J = 0$
- Another axial vector meson: $L = 1, S = 1, J = 1$
- Tensor meson: $L = 1, S = 1, J = 2$

S is the spin, L the internal orbital momentum and $\mathbf{J} = \mathbf{L} + \mathbf{S}$. The production of baryons is not as well understood as that of mesons, and the program includes three different models for it: di-quark, simple popcorn and advanced popcorn.

5 Results

Now we present the results obtained in the simulations. These were carried out in PYTHIA version 8.240, with the tune Monash 2013 [62]. In Fig. 18 the cross section at $\sqrt{s} = 13$ TeV as a function of the dielectron invariant mass is shown. Minimum bias events were simulated, with the same cuts than in [40]: only electrons with a $p_{\perp}$ higher than 0.2 GeV in the range $|\eta| < 0.8$ were selected. To ensure that the events are indeed minimum bias events the option `SoftQCD:inelastic = on` was activated in the code. The contributions of each individual source of dielectron to the spectrum are also plotted, so the blue plots would be the sum of all of these contributions. Is worth noticing that the peaks of some of them like ϕ and J/ψ are much narrower that in the original result, and the low-energy tail is missing. This is due the fact that we have not simulated the transit of these particles through a detector, so our data does not show this Bremsstrahlung effect.

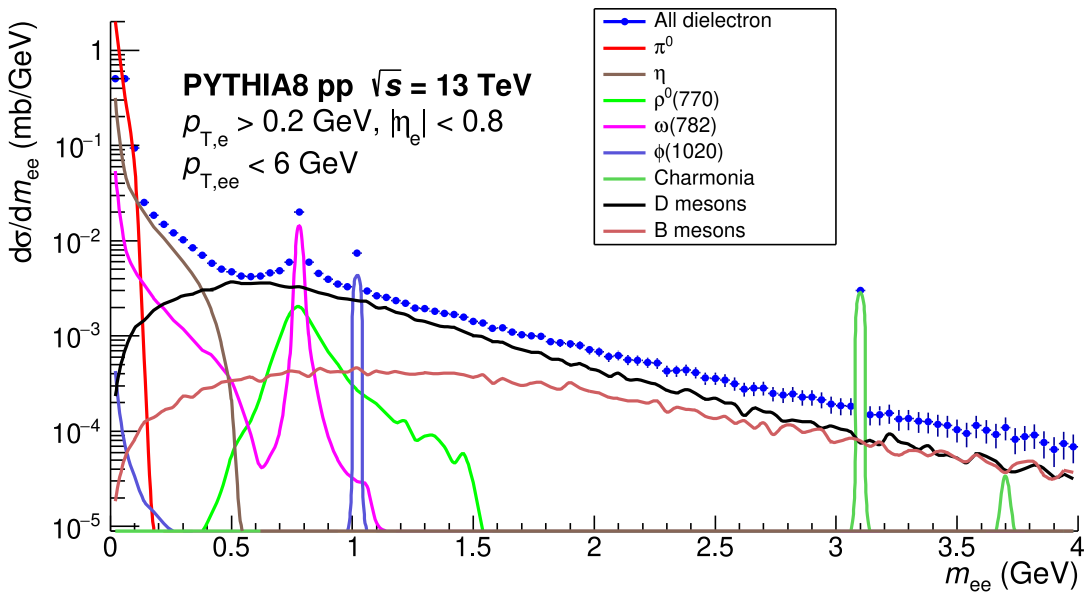

Figure 18: Cross section of dielectron production in pp collisions at $\sqrt{s} = 13$ TeV as a function of the invariant mass.

The transverse momentum $p_{\perp}$ shown in Fig. 19 is also in good agreement with the data. Even if we are more interested in the cross section as a function of the invariant

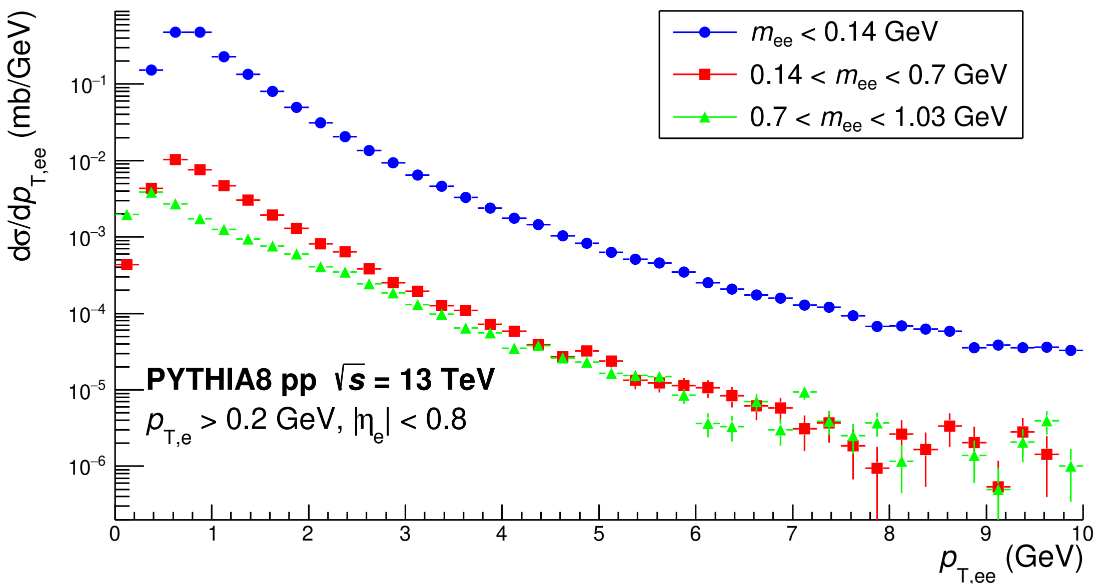

Figure 19: Dielectron cross section as a function of the transverse momentum at $\sqrt{s} = 13$ TeV.

mass, this momentum plots can be used to check if the simulations are doing good, and the results here are also the expected ones. In Fig. 20 is plotted the $p_\perp$ of the mesons that produce dielectron in their decay. The particles with a lower momentum are light mesons (π^0, ρ^0, ω and ϕ) and the charmonium will highlight at higher momentum.

An analysis of the cross section as a function of the charged-particle multiplicity was also conducted. In Fig. 21 the probability of an event having a certain multiplicity at mid-pseudorapidity $|\eta| < 1$ is shown. The probability at $\sqrt{s} = 5.02$ TeV is also displayed, because the multiplicity was also useful to check the healthiness of the simulations. Both distributions are quite similar, reaching higher multiplicities when the energy of the collision is higher. We extracted the mean value of the multiplicity (that is around 13) and represented the cross section for the events with a multiplicity close to this value, lower and higher. The results are plotted in Fig. 22. For low multiplicity the dielectron cross section is lower than the other two cases. The cross sections for mean and high multiplicity are practically the same. This means that actually multiplicity does not affect too much the number of dielectrons produced in a collision. The more number of charged

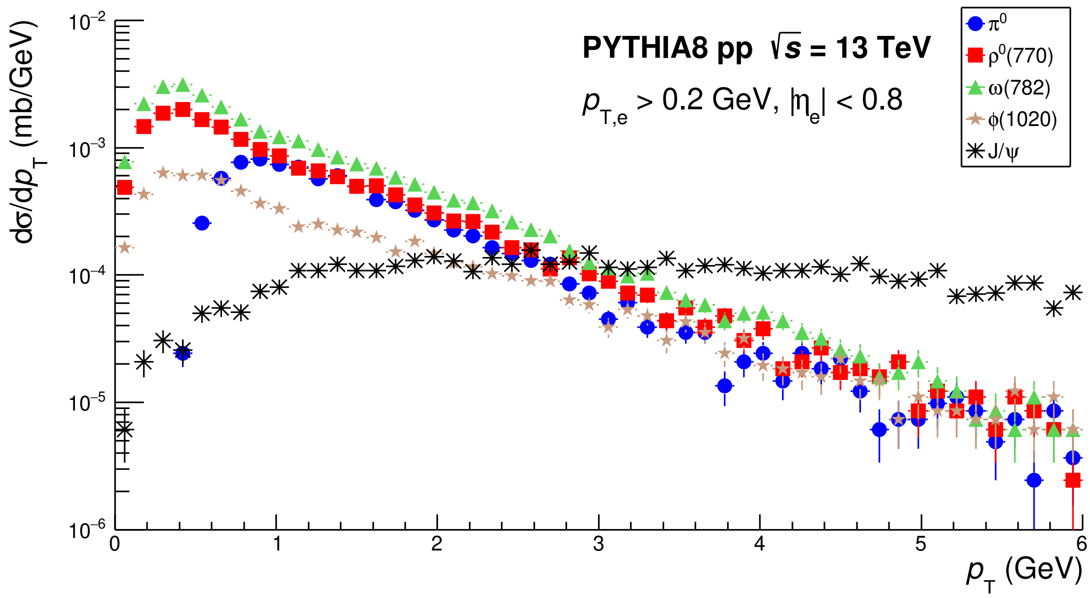

Figure 20: transverse momentum of the light and J/ψ mesons that decay in dielectron.

particles in an event higher is the probability of produce electrons, but because usually in an event there are very few of them the cross sections for mean and high multiplicity are very similar.

5.1 Signal extraction

In the simulations one have a great advantage when collecting the data, since with PYTHIA all the information concerning the creation of particles is available, so one can choose which ones accept and which ones reject with quite freedom. In fact, to draw this plot, just the electron and positron pairs in a single event with the same origin (or related in the case of open mesons) were selected. Of course this information does not exist in a real experiment, so the next thing was trying to imitate the modus operandi of [40]. To do this every electron found in each event was paired. These pairs were classified into same-sign ($N_{\pm\pm}$) and opposite-sign (N_{+-}) pairs. Then the combinatorial background was estimated like in 2.4.1 and extracted from the opposite-sign spectrum. Instead of the geometric mean, the arithmetic mean was the one chosen for the estimation. It was not found any difference in the spectra when using one or the another, and the arithmetic mean is

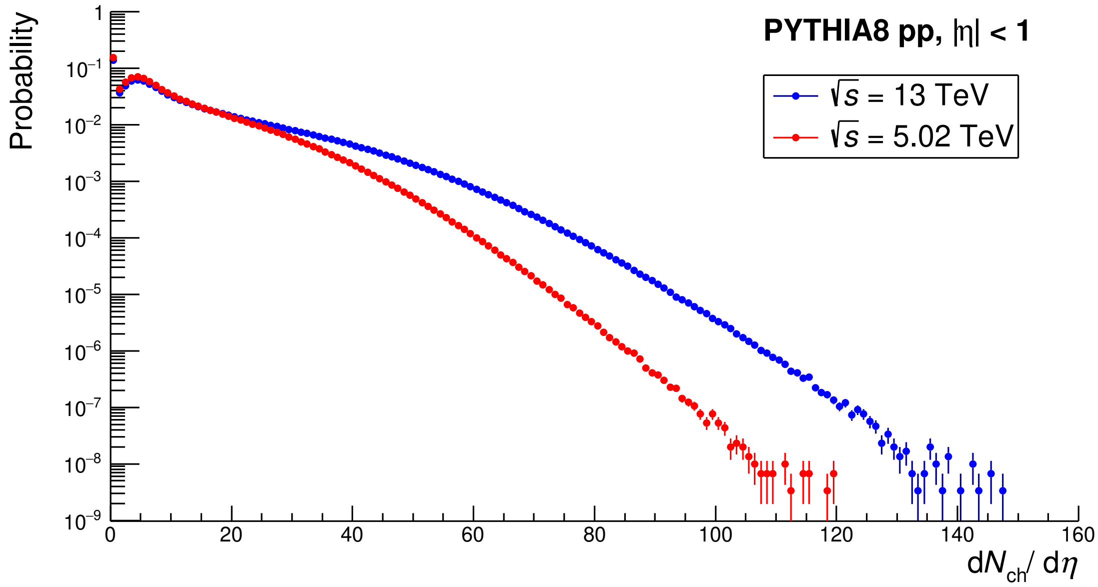

Figure 21: Probability of the charged-particle multiplicity at mid-pseudorapidity $|\eta| < 1$ for two different collision energies.

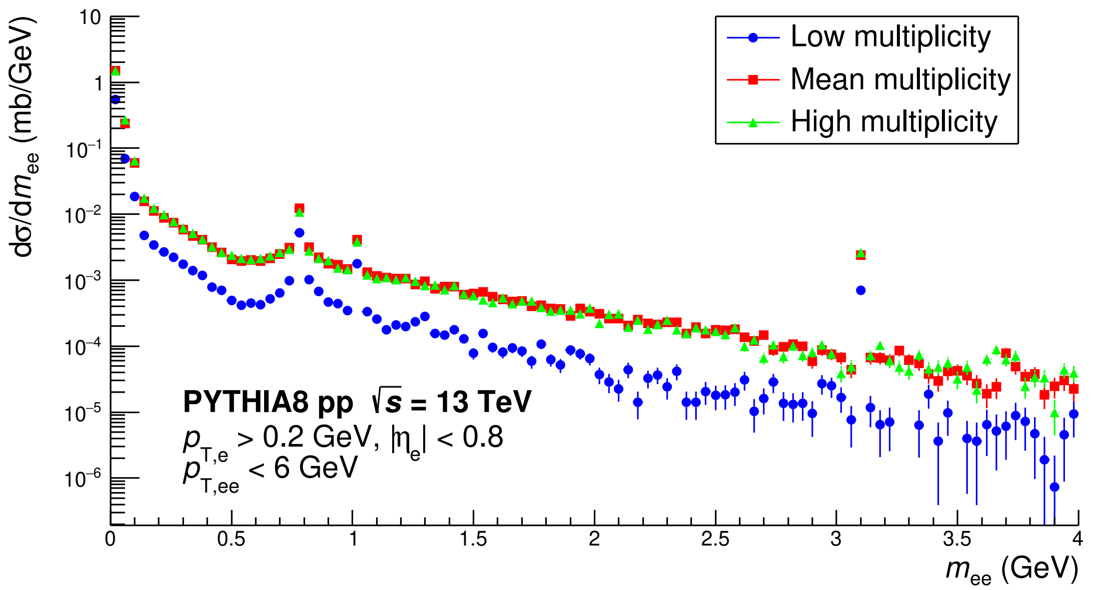

Figure 22: Dielectron cross section for different multiplicity ranges.

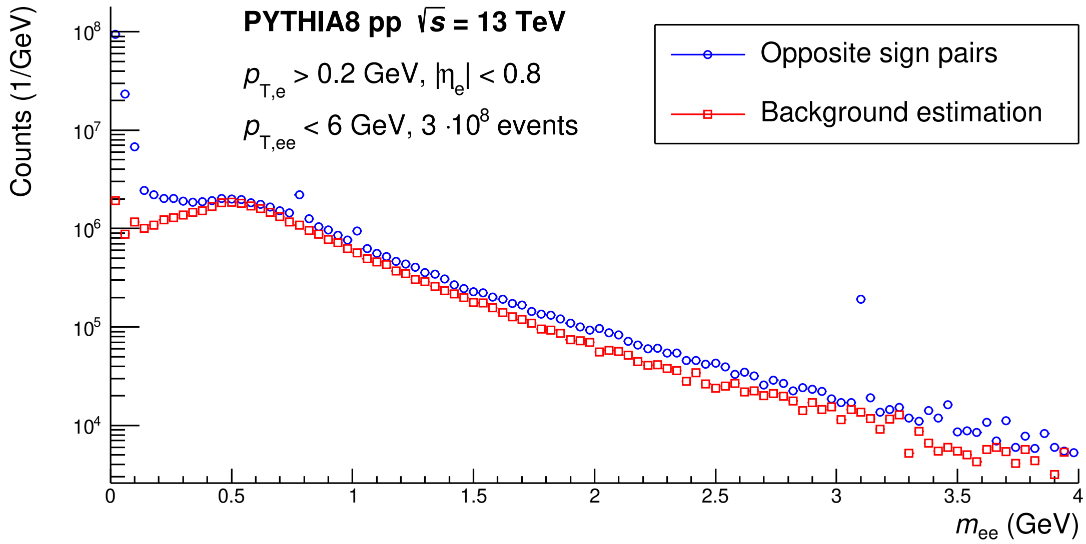

Figure 23: Opposite-sign spectrum and background estimation to extract the actual di-electron signal at $\sqrt{s} = 13$ TeV.

more efficient numerically speaking. Since actual experimental data was not included, the acceptance correction R for opposite and same-sign pairs in the ALICE detector was not considered here. This factor is very close to one and its removal will not affect substantially the final signal. The estimation of the background and the N_{+-} counts are shown in Fig. 23. After extracting the signal and scaling properly to get the cross section the plot in Fig. 24 was obtained.

Now the blue points are the result of extracting the signal, and the coloured lines are the individual contributions expected when selecting the dielectrons "by hand". The spectrum is quite similar as the ones shown before and in agreement with the expected value, just point out the presence of a flatter area in the low mass region, around 0.5 GeV. It looks like the combinatorial background contamination is most likely to appear in that region.

The dielectron cross section as a function of the transverse momentum obtained with this last method is shown in Fig. 25. In this plot is more difficult to see any changes with respect to the invariant mass plot, so in Fig. 26 a comparison between the two methods has been made. Here it appears more clearly the flat area that was not there in the first

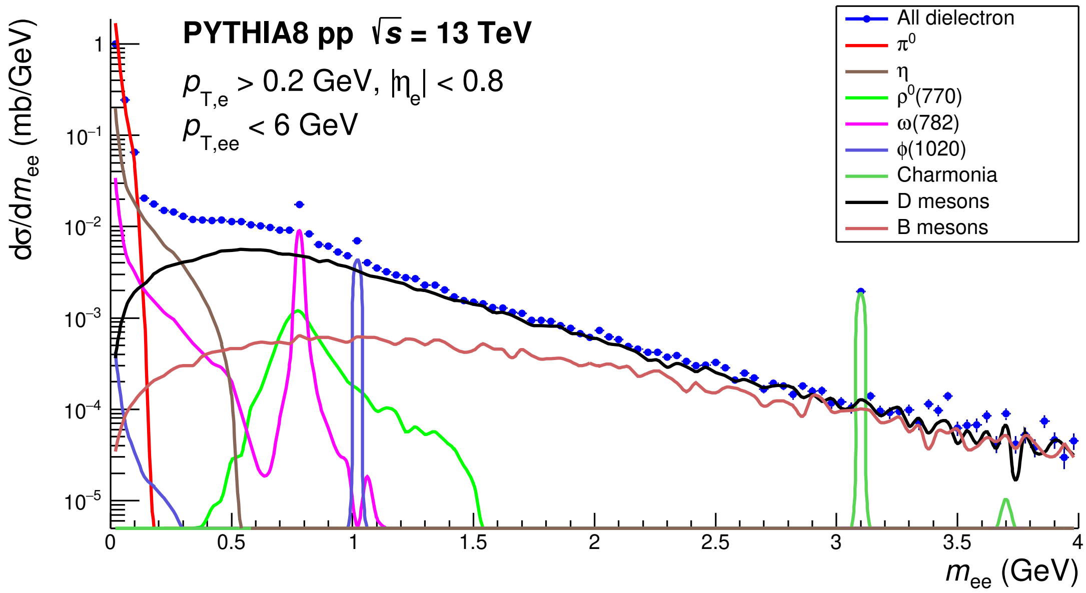

Figure 24: Dielectron cross section as a function of m_{ee} at $\sqrt{s} = 13$ TeV. The same method of signal extraction explained in [40] has been used here.

place. Because of some serious memory problems in the cluster where the simulations have been made there are more events in the first case that in the second method. This is reflected in the bigger statistical fluctuations that can be observed in the region of higher masses. The ratio between these two histograms should be always one, but because of the fluctuations is hard to appreciate this behaviour.

5.2 Pairs from photon conversion

The next thing was adding what would be the equivalent of dielectrons from photo conversion. The numerical method of producing this pairs is inspired by the method used in the program Geant4 [63].

It was considered that a certain fraction of the photons created in an event would give rise to an electron/positron pair, and each one of them would take a random fraction of the energy of the photon $E_{\pm}$. To choose their momenta the function suggested by Urban [64] was used, in which the polar angle is obtained with three random numbers r_1,

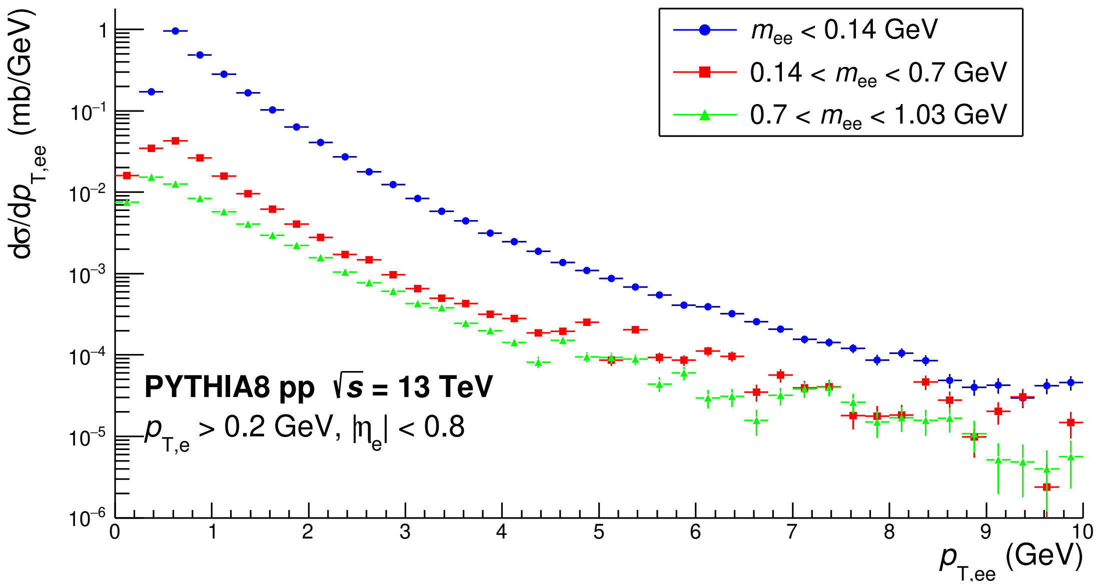

Figure 25: Dielectron cross section as a function of the transverse momentum at $\sqrt{s} = 13$ TeV, using the signal extraction method.

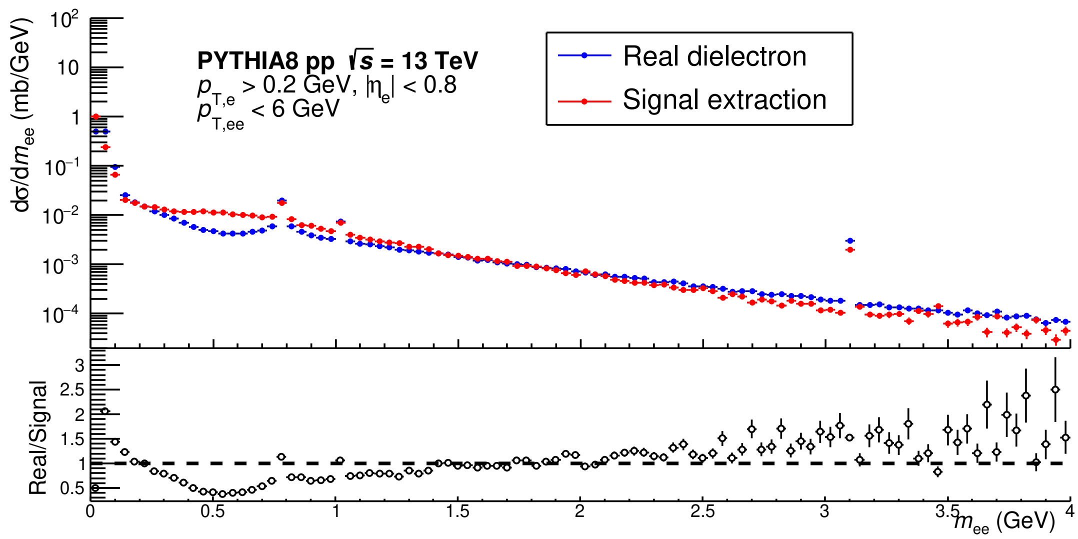

Figure 26: Ratio between the cross section of dielectrons selected "by hand" ("real dielectron" according to the legend) and with the signal extraction method.

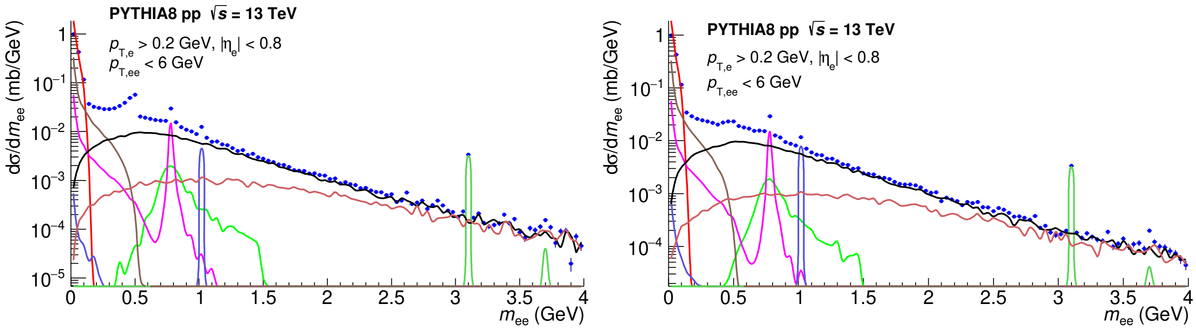

Figure 27: Dielectron cross section with “artificial” photon conversion, contributing 0.06% (left) and 0.006% (right) of all photons.

r_2 and r_3 and the expression

$$\theta_\pm = \frac{m_e}{E_\pm} u, \tag{35}$$

with

$$u = -\frac{\ln r_2 r_3}{a} \quad \text{if} \quad r_1 < \frac{9}{9+d} \tag{36}$$

and

$$u = -\frac{\ln r_2 r_3}{3a} \quad \text{else}, \tag{37}$$

being $a = 5/8$ and $d = 27$. e^+ and e^- are considered coplanar with the parent direction, and the azimuthal angle ϕ is generated isotropically. With this information and the energy conservation the vector of the electron momentum is generated, to be later rotated to the global reference system.

In Fig. 27 the result of adding these artificial pairs is shown. In the first case (left) it was considered that only 6% of photon conversion pairs were remaining after the first selection cut on the ITS. Then, thanks to the selection of the angle with the magnetic field, only the 1% left survived, so this probability of 0.06% were chosen to decided whether a photon would produce a pair or not. A strange bump can be seen around 0.5 GeV, telling that this probability is way too high. After reducing it by an order of magnitude (right) a small fraction of this bump is still remaining.

The reason why the shape of this points and why they appear at that invariant mass is not fully understood. One certain conclusion is that the rejection methods used for photon conversion pairs in real experimental data are very effective.

The same simulations have been also made for a collision energy of $\sqrt{s}$ =5.02 TeV. This is because there are some interesting publications in which the dielectron cross section in *p-p* collisions is studied [36], to then compare it to the cross section at the same energy but for *p-Pb* collisions. So here it can be found our version of the same spectrum. The results can bee seen in Fig. 28.

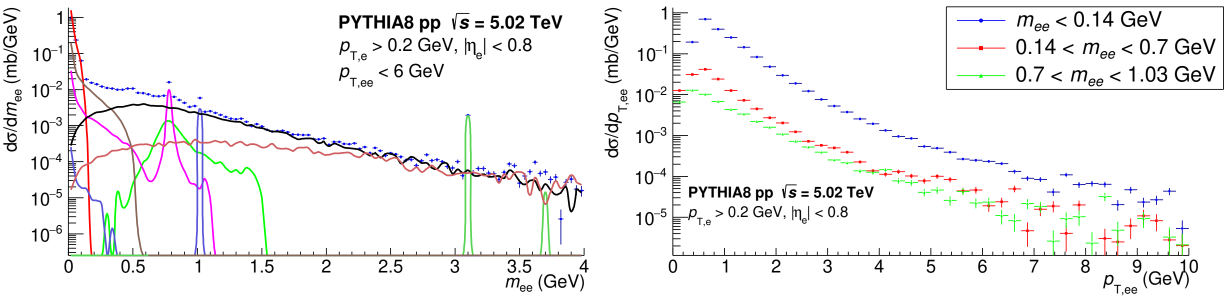

Figure 28: Dielectron cross section as a function of the invariant mass (left) and the transverse momentum (right) for $\sqrt{s}$ = 5.02 TeV.

Both cross sections are very similar to the ones at $\sqrt{s}$ = 13 TeV, only a little reduced as expected. In Fig. 29 a comparison between these two energies is shown. The ratio should be the same regardless of the invariant mass, but because the big fluctuations at the end of the plot this behaviour is difficult to identify.

The results of the simulations at this energy with the other two considered cases can be seen at Appendix A.

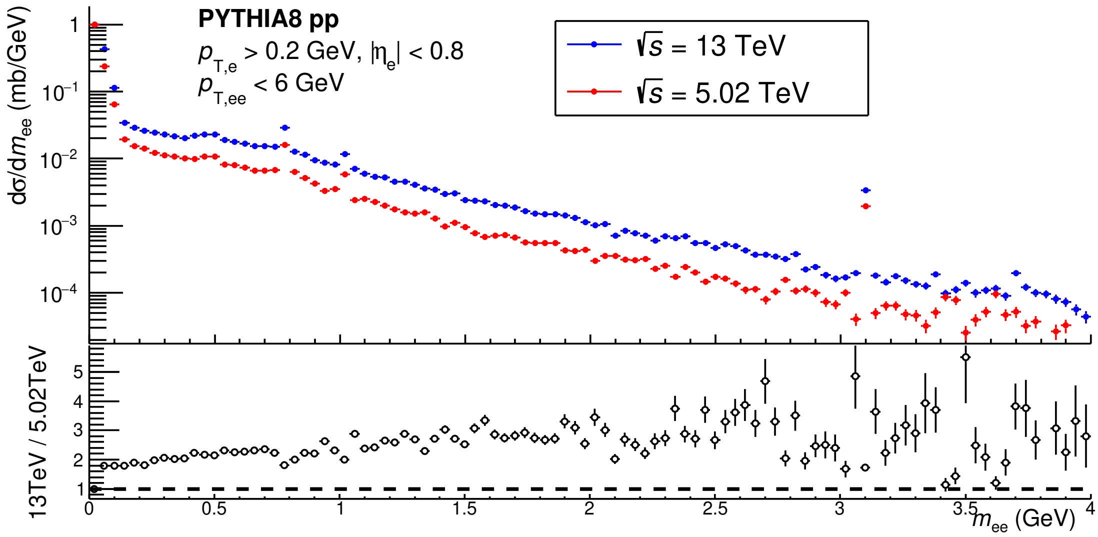

Figure 29: Ratio between the cross section of dielectrons at two different energies. The cross section is lower when the energy is reduced.

6 Conclusions and outlook

The dielectron cross section as a function of the invariant mass and the transverse momentum has been simulated for a couple of collision energies. The results are the expected according to the real experimental data, only with little discrepancies due to the fact that a Monte Carlo simulation of the detector has not been conducted. Two ways of obtain this cross section have been tried: using the information provided directly by PYTHIA, selecting only the real dielectron candidates, and with the signal extraction methods for real life situations. A small difference in the low mass region appeared when using the signal extracting method, suggesting that the background coming from there is more likely to show up around that region.

Because with PYTHIA these effects can not be simulated, the possible photon conversion pairs that can affect the plots were included artificially. To do this, the code of this process found in Geant4 was adapted to the codes in PYTHIA. Trying different amounts of photon conversion pairs an alteration of the signal around 0.5 GeV was found. The conclusion was that the methods followed with real experimental data to eliminate the contribution of these pairs are really effective, but the reason why they appear in that region is not fully understood.

The results were very similar for the two collisions energies presented here, except for an expected reduction of the cross section value when the energy is smaller. No other differences were found between the two situations.

One thing that can be made for the benefit of this topic is to performance a Monte Carlo simulation of the behaviour of ALICE to this data. It would help to understand better the response of the detector and to be more confident when comparing the simulations to the experimental data. Another thing that can be made is to repeat the simulations with a larger number of events, to reduce the fluctuations found at some points that made more difficult the task of coming to conclusions. A suggestion for future investigations is to conduct the simulations for proton-lead or even lead-lead collisions, because it would help the understanding of the leptonic production in these collisions and, therefore, in the QGP.

A Simulations at $\sqrt{s} = 5.02$ TeV

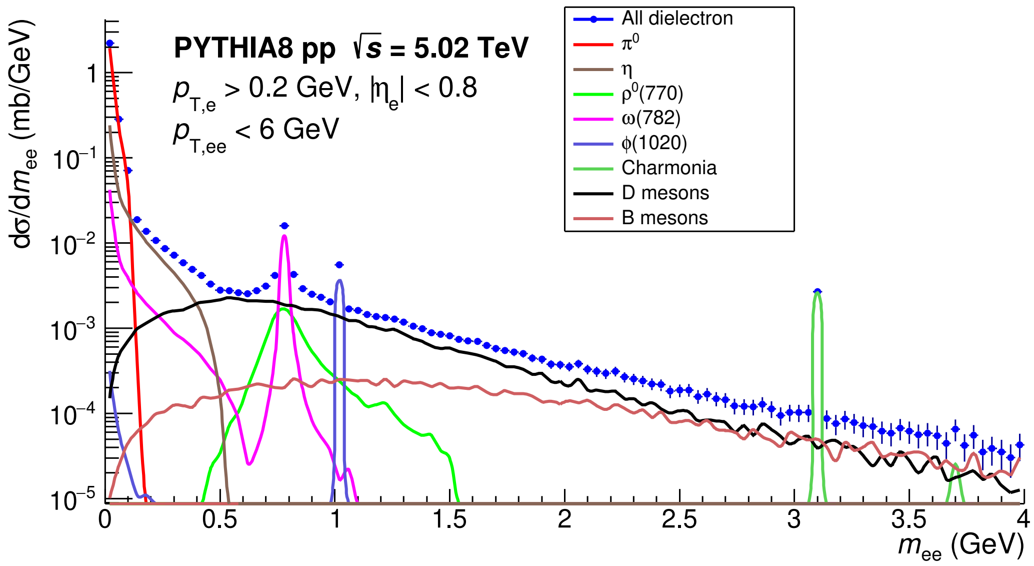

Figure 30: $\mathrm{d}\sigma/\mathrm{d}m_{\mathrm{ee}}$ at $\sqrt{s} = 5.02$ TeV, dielectron selected “by hand”.

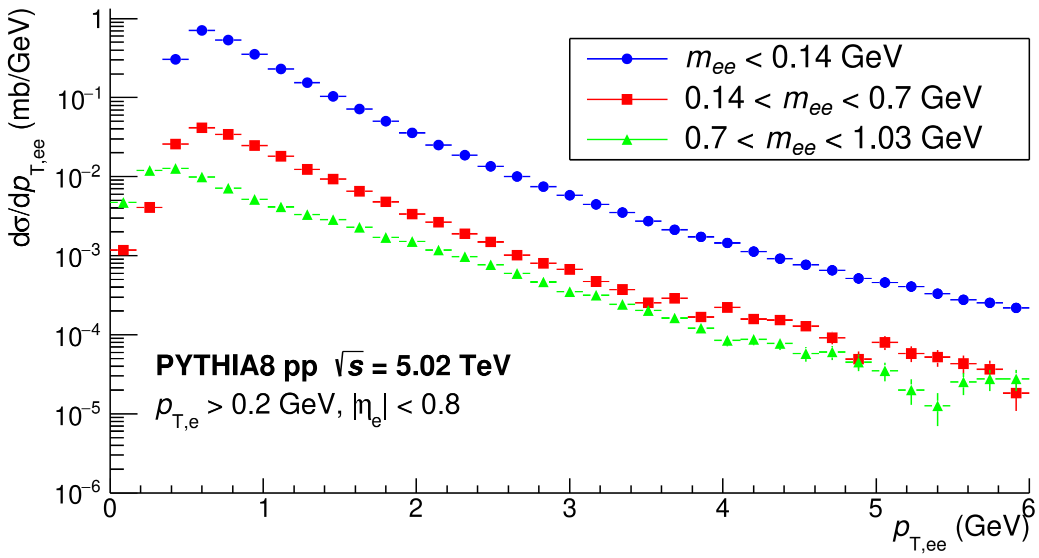

Figure 31: $\mathrm{d}\sigma/\mathrm{d}m_{\perp,\mathrm{ee}}$ at $\sqrt{s} = 5.02$ TeV, dielectron selected “by hand”.

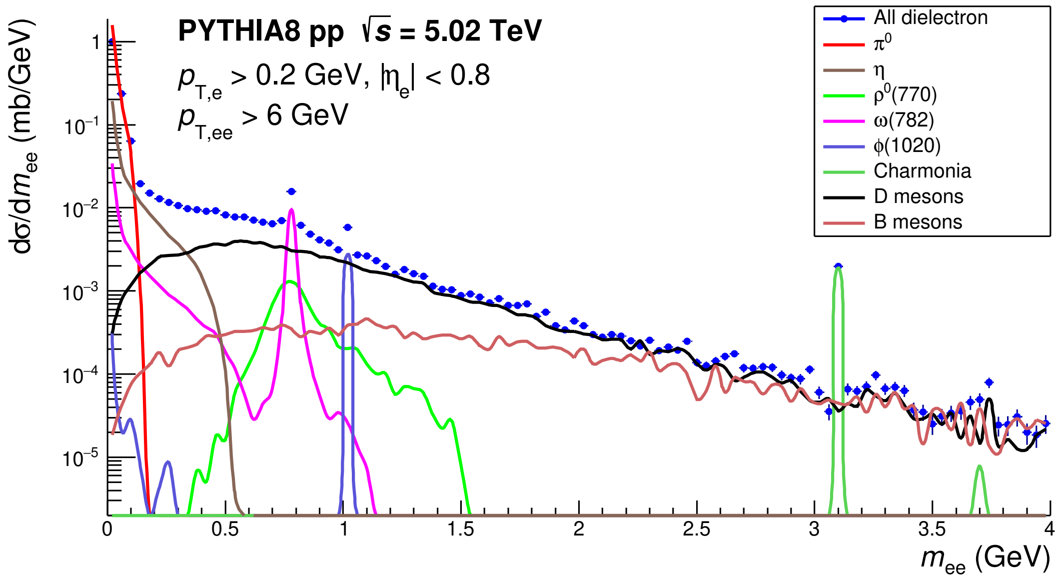

Figure 32: $\mathrm{d}\sigma/\mathrm{d}m_{\mathrm{ee}}$ at $\sqrt{s} = 5.02$ TeV, signal extraction method.

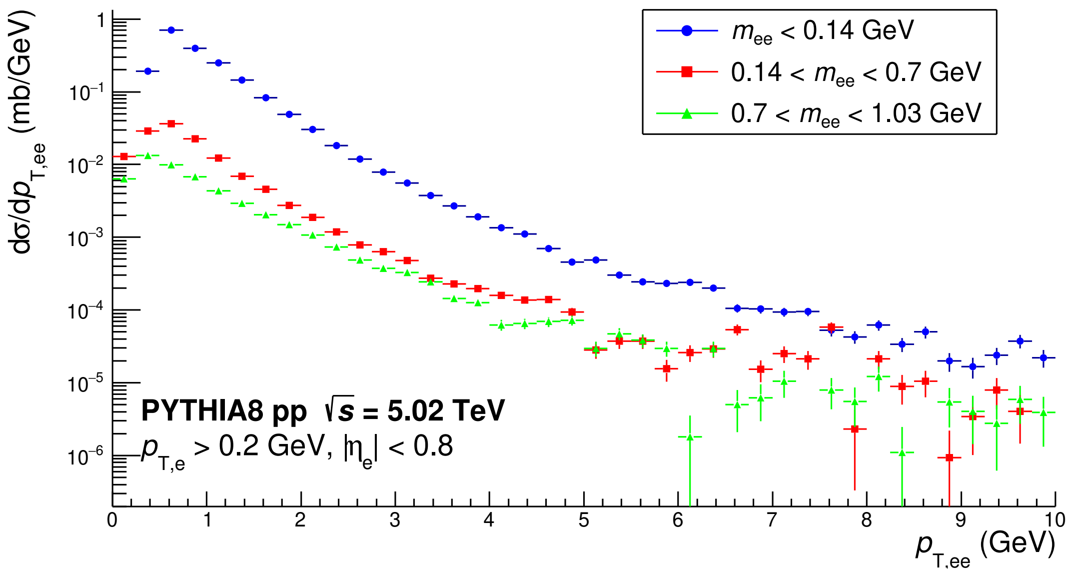

Figure 33: $\mathrm{d}\sigma/\mathrm{d}m_{\perp,\mathrm{ee}}$ at $\sqrt{s} = 5.02$ TeV, signal extraction method.

References

[1] Shreyasi Acharya, D Adamová, J Adolfsson, MM Aggarwal, G Aglieri Rinella, M Agnello, N Agrawal, Z Ahammed, SU Ahn, S Aiola, et al. Dielectron production in proton-proton collisions at $\sqrt{s} = 7$ TeV. *Journal of High Energy Physics*, 2018(9):64, 2018.

[2] J-E Augustin, Adam M Boyarski, Martin Breidenbach, F Bulos, JT Dakin, GJ Feldman, GE Fischer, D Fryberger, G Hanson, B Jean-Marie, et al. Discovery of a narrow resonance in e+ e- annihilation. *Physical Review Letters*, 33(23):1406, 1974.

[3] Franz Mandl and Graham Shaw. *Quantum field theory*. John Wiley & Sons, 2010.

[4] David Griffiths. *Introduction to elementary particles*. John Wiley & Sons, 2008.

[5] Francis Halzen and Alan D Martin. *Quark & Leptons: An Introductory Course In Modern Particle Physics*. John Wiley & Sons, 2008.

[6] Alfred S Goldhaber and Michael Martin Nieto. Mass of the graviton. *Physical Review D*, 9(4):1119, 1974.

[7] Marcela Carena and Howard E Haber. Higgs boson theory and phenomenology. *Progress in Particle and Nuclear Physics*, 50(1):63–152, 2003.

[8] Review of the Universe. Quantum Field Theory. The Standard Model. `http://universe-review.ca/R15-12-QFT16.htm`. Accessed: 2020-09-14.

[9] MissMJ and Cush. Standard Model of Elementary Particles. `https://commons.wikimedia.org/w/index.php?curid=4286964`. Accessed: 2020-08-30.

[10] Ernest M Henley and Alejandro García. *Subatomic Physics*. World Scientific Publishing, 2007.

[11] Brian R Martin and Graham Shaw. *Particle physics*. John Wiley & Sons, 2017.

[12] Wolfgang Pauli. Letter to the Physical Institute of the Federal Institute of Technology. Zunch, 1930.

[13] Chien-Shiung Wu, Ernest Ambler, RW Hayward, DD Hoppes, and Ralph Percy Hudson. Experimental test of parity conservation in beta decay. *Physical review*, 105(4):1413, 1957.

[14] CERN Press Off. CERN experiments observe particle consistent with long-sought Higgs boson, 2012.

[15] Silvia Ferreres-Solé and Torbjörn Sjöstrand. The space-time structure of hadronization in the Lund model. *The European Physical Journal C*, 78(11):1–23, 2018.

[16] JF Grosse-Oetringhaus. *Measurement of the charged-particle multiplicity in proton-proton collisions with the ALICE detector PhD Thesis University of Münster CERN*. PhD thesis, THESIS-2009-033, 2009.

[17] Christian Klein-Bösing. Study of the quark-gluon plasma with hard and electromagnetic probes. *Habilitation dissertation, Westfälischen Wilhelms-Universität Münster*, 2013.

[18] Raghunath Sahoo. Relativistic kinematics. *arXiv preprint arXiv:1604.02651*, 2016.

[19] Ed Daw. Lecture 7: Rapidity and pseudorapidity. *http://www.hep.shef.ac.uk/edaw/PHY206/Site/2012_course_files/phy206rlec7.pdf*, 2012.

[20] Cheuk-Yin Wong. *Introduction to high-energy heavy-ion collisions*. World scientific, 1994.

[21] John C Collins, Davison E Soper, and George Sterman. Factorization of hard processes in QCD. In *Perturbative QCD*, pages 1–91. World Scientific, 1989.

[22] Peter Skands. Introduction to QCD. In *Searching for New Physics at Small and Large Scales: TASI 2012*, pages 341–420. World Scientific, 2013.

[23] Ringaile Placakyte. Parton distribution functions. *arXiv preprint arXiv:1111.5452*, 2011.

[24] Mark Thomson. *Modern particle physics*. Cambridge University Press, 2013.

[25] Richard D Ball, Valerio Bertone, Stefano Carrazza, Luigi Del Debbio, Stefano Forte, Patrick Groth-Merrild, Alberto Guffanti, Nathan P Hartland, Zahari Kassabov, José I Latorre, et al. Parton distributions from high-precision collider data. *The European Physical Journal C*, 77(10):663, 2017.

[26] Steffen Georg Weber. *Multiplicity dependent J/ψ production in proton-proton collisions at the LHC*. PhD thesis, Darmstadt, 2018.

[27] Betty Abelev, J Adam, D Adamová, AM Adare, MM Aggarwal, G Aglieri Rinella, AG Agocs, A Agostinelli, S Aguilar Salazar, Z Ahammed, et al. Measurement of inelastic, single-and double-diffraction cross sections in proton–proton collisions at the LHC with ALICE. *The European Physical Journal C*, 73(6):2456, 2013.

[28] Jan Fiete Grosse-Oetringhaus and Klaus Reygers. Charged-Particle Multiplicity in Proton–Proton Collisions. *Journal of Physics G: Nuclear and Particle Physics*, 37(8):083001, 2010.

[29] Richard P Feynman. Very high-energy collisions of hadrons. *Physical Review Letters*, 23(24):1415, 1969.

[30] Z Koba, Holger Bech Nielsen, and P Olesen. Scaling of multiplicity distributions in high energy hadron collisions. *Nuclear Physics B*, 40:317–334, 1972.

[31] William A Zajc. KNO scaling isn't what it used to be. *Physics Letters B*, 175(2):219–222, 1986.

[32] GJS Ross and DA Preece. The negative binomial distribution. *Journal of the Royal Statistical Society: Series D (The Statistician)*, 34(3):323–335, 1985.

[33] GJ Alner, K Alpgård, P Anderer, RE Ansorge, B Åsman, K Böckmann, CN Booth, L Burow, P Carlson, J-L Chevalley, et al. Multiplicity distributions in different pseudorapidity intervals at a CMS energy of 540 GeV. *Physics Letters B*, 160(1-3):193–198, 1985.

[34] Alberto Giovannini and R Ugoccioni. Possible scenarios for soft and semihard component structure in central hadron-hadron collisions in the TeV region. *Physical Review D*, 59(9):094020, 1999.

[35] Georges Aad, B Abbott, J Abdallah, B Abeloos, R Aben, M Abolins, OS AbouZeid, NL Abraham, H Abramowicz, et al. Charged-particle distributions in $\sqrt{s} = 13$ TeV pp interactions measured with the ATLAS detector at the LHC. *Physics Letters B*, 758:67–88, 2016.

[36] Shreyasi Acharya, Dagmar Adamova, Alexander Adler, Jonatan Adolfsson, Madan Mohan Aggarwal, Gianluca Aglieri Rinella, Michelangelo Agnello, Neelima Agrawal, Zubayer Ahammed, Shakeel Ahmad, et al. Dielectron production in proton-proton and proton-lead collisions at $\sqrt{s_{NN}} = 5.02$ TeV. *arXiv preprint arXiv:2005.11995*, 2020.

[37] Andrew Adare, S Afanasiev, C Aidala, NN Ajitanand, Y Akiba, H Al-Bataineh, J Alexander, K Aoki, L Aphecetche, R Armendariz, et al. Dilepton mass spectra in p+ p collisions at $\sqrt{s_{NN}} = 200$ GeV and the contribution from open charm. *Physics Letters B*, 670(4-5):313–320, 2009.

[38] Andrew Adare, S Afanasiev, C Aidala, NN Ajitanand, Y Akiba, H Al-Bataineh, J Alexander, A Al-Jamel, K Aoki, Laurent Aphecetche, et al. Detailed measurement of thee^+e^- pair continuum in p+ p and au+ au collisions at $\sqrt{s_{NN}} = 200$ GeV and implications for direct photon production. *Physical Review C*, 81(3):034911, 2010.

[39] L Adamczyk, G Agakishiev, MM Aggarwal, Z Ahammed, AV Alakhverdyants, I Alekseev, J Alford, BD Anderson, CD Anson, D Arkhipkin, et al. Di-electron spectrum at mid-rapidity in p+ p collisions at $\sqrt{s_{NN}} = 200$ GeV. *Physical Review C*, 86(2):024906, 2012.

[40] Shreyasi Acharya, Fernando Torales-Acosta, Dagmar Adamová, Jonatan Adolfsson, Madan M Aggarwal, G Aglieri Rinella, Michelangelo Agnello, Nikita Agrawal, Zubayer Ahammed, Sang Un Ahn, et al. Dielectron and heavy-quark production in inelastic and high-multiplicity proton–proton collisions at $\sqrt{s} = 13$ TeV. *Physics Letters B*, 788:505–518, 2019.

[41] Amand Faessler and Christian Fuchs. Medium dependence of vector meson properties in heavy ion collisions. *Romanian Reports in Physics*, 59(2):419, 2007.

[42] Torsten Dahms. Dilepton spectra in p+ p and Au+ Au collisions at RHIC. *arXiv preprint arXiv:0810.3040*, 2008.

[43] Sebastian Lehner. *Dielectron production and a search for highly-charged particles in Pb–Pb collisions*. PhD thesis, Austrian Academy of Sciences (AT), 2019.

[44] Betty Abelev, J Adam, D Adamová, AM Adare, MM Aggarwal, G Aglieri Rinella, M Agnello, AG Agocs, A Agostinelli, Z Ahammed, et al. Energy dependence of the transverse momentum distributions of charged particles in pp collisions measured by alice. *The European Physical Journal C*, 73(12):2662, 2013.

[45] B Abelev, J Adam, D Adamová, MM Aggarwal, G Aglieri Rinella, M Agnello, A Agostinelli, N Agrawal, Z Ahammed, N Ahmad, et al. Production of charged pions, kaons and protons at large transverse momenta in pp and Pb–Pb collisions at $\sqrt{s_{\mathrm{NN}}} = 2.76$ TeV. *Physics Letters B*, 736:196–207, 2014.

[46] Lucas Altenkämper, Friederike Bock, Constantin Loizides, and Nicolas Schmidt. Applicability of transverse mass scaling in hadronic collisions at energies available at the CERN Large Hadron Collider. *Physical Review C*, 96(6):064907, 2017.

[47] Kenneth Aamodt, A Abrahantes Quintana, R Achenbach, S Acounis, D Adamová, C Adler, M Aggarwal, F Agnese, G Aglieri Rinella, Z Ahammed, et al. The ALICE experiment at the CERN LHC. *Journal of Instrumentation*, 3(08):S08002, 2008.

[48] Arturo Tauro. ALICE Schematics during RUN2 - with description. CERN Document Server, 2017.

[49] Walter Blum, Werner Riegler, and Luigi Rolandi. *Particle detection with drift chambers*. Springer Science & Business Media, 2008.

[50] First results of the ALICE detector performance at 13 TeV. Aug 2015.

[51] Torbjörn et al. Sjöstrand. An introduction to PYTHIA 8.2. *Computer Physics Communications*, 191:159–177, Jun 2015.

[52] Torbjörn Sjöstrand. Status and developments of event generators. 2016, 1608.06425.

[53] Torbjörn Sjöstrand and Maria van Zijl. A multiple-interaction model for the event structure in hadron collisions. *Phys. Rev. D*, 36:2019–2041, Oct 1987.

[54] Stefan Höche. Introduction to parton-shower event generators. In *Journeys Through the Precision Frontier: Amplitudes for Colliders: TASI 2014 Proceedings of the 2014 Theoretical Advanced Study Institute in Elementary Particle Physics*, pages 235–295. World Scientific, 2016.

[55] Torbjörn Sjöstrand, Stephen Mrenna, and Peter Skands. PYTHIA 6.4 physics and manual. *Journal of High Energy Physics*, 2006(05):026, 2006.

[56] T. Sjostrand and P. Skands. Multiple Interactions and Beam Remnants. 2004, hep-ph/0401060.

[57] Spyros Argyropoulos and Torbjörn Sjöstrand. Effects of color reconnection on $t\bar{t}$ final states at the LHC. *Journal of High Energy Physics*, 2014(11):43, 2014.

[58] Torbjörn Sjöstrand. Colour reconnection and its effects on precise measurements at the LHC. 2013, 1310.8073.

[59] Gösta Gustafson. Multiple Interactions, Saturation, and Final States in pp Collisions and DIS. 2009, 0905.2492.

[60] Torbjörn Sjöstrand. Jet fragmentation of multiparton configurations in a string framework. *Nucl. Phys. B*, 248:469–502, 1984.

[61] Bo Andersson, Gösta Gustafson, Gunnar Ingelman, and Torbjörn Sjöstrand. Parton fragmentation and string dynamics. *Physics Reports*, 97(2-3):31–145, 1983.

[62] Peter Skands, Stefano Carrazza, and Juan Rojo. Tuning PYTHIA 8.1: the Monash 2013 tune. *The European Physical Journal C*, 74(8):1–39, 2014.

[63] GEANT Collaboration et al. Physics reference manual. *Version: geant4*, 9(0), 2016.

[64] Rene Brun, L Urban, Federico Carminati, Simone Giani, M Maire, A McPherson, F Bruyant, and G Patrick. GEANT: detector description and simulation tool. Technical report, CERN, 1993.

List of Figures

Plagiatserklärung

Hiermit versichere ich, dass die vorliegende Arbeit über **Dielectron production in p-p collisions with PYTHIA8 event generator** selbstständig verfasst worden ist, dass keine anderen Quellen und Hilfsmittel als die angegebenen benutzt worden sind und dass die Stellen der Arbeit, die anderen Werken - auch elektronischen Medien - dem Wortlaut oder Sinn nach entnommenen wurdem, auf jeden Fall unter Angabe der Quelle als Entlehnung kenntlich gemacht worden sind.

Ich erkläre mich mit einem Abgleich der Arbeit mit anderen Texten zwecks Auffindung von Übereinstimmungen sowie mit einer zu diesem Zweck vorzunehmenden Speicherung der Arbeit in eine Datebank einverstanden.
